Cytoskeleton regulators CAPZA2 and INF2 associate with CFTR to control its membrane levels under EPAC1 activation

João D. Santos[1], Francisco R. Pinto[1], Margarida D. Amaral[1], Manuela Zaccolo[2], Carlos M. Farinha[1*]

[1] BioISI-Biosystems and Integrative Sciences Institute, Faculdade de Ciências da Universidade de Lisboa, Campo Grande 1749-016 Lisboa, Portugal
[2] Department of Physiology, Anatomy & Genetics, University of Oxford, Oxford OX1 3PT, UK
*corresponding author

Abstract (100-250 words; 227)

Cystic Fibrosis (CF), the most common lethal autosomic recessive disorder among Caucasians, is caused by mutations in the gene encoding the Cystic Fibrosis Transmembrane conductance Regulator (CFTR) protein, a cAMP-regulated chloride channel expressed at the apical surface of epithelial cells. cAMP regulates both CFTR channel gating through a protein kinase A (PKA)-dependent process and plasma membane (PM) stability through activation of the exchange protein directly activated by cAMP1 (EPAC1). This cAMP effector, when activated promotes the interaction NHERF1:CFTR leading to an increase CFTR PM by decreasing its endocytosis. Here, we used protein interaction profiling and bioinformatic analysis to identify proteins that interact with CFTR under EPAC1 activation as possible regulators of CFTR PM anchoring.

We identified an enrichment in cytoskeleton related proteins among which we characterized CAPZA2 and INF2 as regulators of CFTR trafficking to the PM. We found that CAPZA2 promotes wt-CFTR trafficking under EPAC1 activation at the PM whereas a reduction of INF2 levels leads to a similar trafficking promotion effect. These results suggest that CAPZA2 is a positive regulator and INF2 a negative one for the increase of CFTR at the PM after an increase of cAMP and concomitant activation of EPAC1. Identifying the specific interactions involving CFTR and elicited by EPAC1 activation provides novel insights into CFTR trafficking, insertion and/or stabilization at the PM and highlighs new potential therapeutic targets to tackle CF disease.

Keywords (max 6) CFTR; EPAC1; cAMP; Actin cytoskeleton

1. Introduction

Cystic Fibrosis (CF) is the most common lethal and life-limiting autosomic recessive disorder among Caucasian population, affecting about 1 in 2500-6000 new borns [1] and it is caused by dysfunction of the Cystic Fibrosis Transmembrane Conductance Regulator (CFTR) protein. CFTR protein is a member of the ABC (ATP-binding cassette) transporter superfamily and functions as a cAMP-regulated chloride and bicarbonate channel in the apical membrane of epithelial cells to maintain ion and fluid homeostasis [2,3]. CFTR is composed by two membrane spanning domains (MSD1 and MSD2), forming the pore of the channel; two cytosolic nucleotide binding domains (NBD1 and NBD2), where ATP is hydrolysed regulating channel gating and one CFTR-exclusive regulatory domain (RD) that contains multiple phosphorylation sites essential for channel activity [4]

The most common CF-causing mutation corresponds to a deletion of phenylalanine (Phe) position 508 in NBD1 (F508del) and occurrs in approximately 85% of CF patients in at least one allele and leads to CFTR misfolding and ER retention. The mutant protein is prematurely degraded precluding its delivery to the cell surface [3].

The levels of CFTR at the PM are determined by a balance between three main processes - CFTR anterograde transport, CFTR endocytosis and CFTR recycling [5,6] – all of which rely on CFTR interaction with several proteins among which PDZ domain-containing proteins (PDZ proteins) play an essential role. NHERF1 anchors CFTR at the PM and to the actin cytoskeleton [5,7]. In the PDZ-dependent CFTR-NHERF1 complex, NHERF1 interacts with ezrin and this NHERF1-ezrin interaction locks CFTR in an immobile and actin-tethered complex preventing its endocytosis [8,9]. NHERF1 not only regulates wt-CFTR at the PM but it is also a key factor in F508del-CFTR stability at the PM by protecting it from lysosomal degradation [10]. Recently, it was shown that activation of the exchange protein directly activated by cAMP 1 (EPAC1) promotes its interaction with NHERF1 and CFTR, leading to an increase of CFTR at the PM [11].

EPAC proteins function as GEF for both Rap1 and Rap2 [12] and are involved in the regulation of cell-cell and cell-matrix adhesion, cytoskeleton rearrangements and cell polarization [13]. Upon activation with cAMP, EPAC1 – the major EPAC expressed in the lung [14] is targeted to the PM where it tethers to phosphatidic acid or to phosphorylated ERM proteins inducing its downstream effectors such as Rap [15]. Identification of NHERF1-dependent CFTR-EPAC1 interaction [11] highlighted a two-level regulation of the channel by cAMP – low concentrations of cAMP activate PKA to regulate CFTR function whereas high cAMP levels promote EPAC1-dependent regulation of PM levels [11].

Recently, it was also reported that EPAC1 plays an important role in Cl^- secretion not only through CFTR) but also through TMEM16A, a Ca^{2+} dependent Cl^- channel [16]. Activation of EPAC1 by cAMP, activates Rap2 leading to an increase in Ca^{2+} [17]. Thus, EPAC1 appears as a hub in the cAMP/Ca^{2+} crosstalk, also activating TMEM16A. Despite these recent advances the mechanism and the macromolecular complexes elicited at the PM by EPAC1 activation are still largely uncharacterized.

Here, we used a proteomic interaction profiling approach coupled to global bioinformatic analysis to identify specific CFTR interactions elicited by EPAC1 activation. We identified several novel interactors and characterized two involved in its anchoring at the PM, CAPZA2 and INF2. Our data show that when CAPZA2 is downregulated, the effect of EPAC1 on wt-CFTR PM levels is boosted. On the other hand, when INF2 is downregulated, the opposite effected is observed - reduced levels of wt-CFTR at the PM. We report here for the first time the acting cytoskeleton dynamics regulators CAPZA2 and INF2 as modulators of CFTR anchoring at the PM.

Considering that the therapeutic opportunities of restoring CFTR PM stability are still poorly explored, characterization of the molecular mechanism of CFTR anchoring as provided here may contribute to identify novel targets that can be used in combination with other therapeutic strategies.

2. Materials and methods

2.1. Cell culture and compound treatment

Parental CFBE41o- cells and CFBE stably transduced with wt-CFTR were grown in EMEM (Lonza, #BE12-611F) supplemented with 10% (v/v) FBS (GIBCO® Life Technologies, #10270-106) and 5 µg/ml puromycin (Sigma, #P8833). CFBE41o- cells expressing double tagged mCherry-FLAG-wt-CFTR, under a doxycycline inducible promoter were grown in DMEM with 4.5 g/L Glucose and L-Glutamine supplemented with 10% (v/v) FBS, 2 µg/ml puromycin and 10µg/ml blasticidin (InvivoGen, #ant-bl). CFTR expression was induced with doxycycline 1 µg/ml (Sigma #9891) for 24h. All cell lines were grown at 37ºC in 5% CO2.

When applicable, cells were treated 2h with 1 µM 8-pCPT-2′-O-Me-cAMP-AM (007-AM) (BioLog, #c041-05), 10 µM forskolin or vehicle control (DMSO) in the appropriate serum-free media.

2.2. CFTR immunoprecipitation

CFTR was immunoprecipitated from stable CFBE41o- cells expressing wt-CFTR previously treated with the in vivo cross link agent dithiobis(succinimidylpropinate) (DSP) (Thermo Scientific, #22585). Parental CFBE cells (not expressing CFTR) were used to define the background. Immunopreciptiation was performed using the anti-CFTR 596 monoclonal antibody coupled to rProtein G agarose beads coupled with the 596 as previously described (Canato et al 2018; Santos et al 2019). Cell lysis was performed for 30 min with Triton lysis buffer (TBS) (25 mM Tris-HCl pH 7.4, 150 mM $NaCl_2$, 1% (v/v) Triton-X 100, supplemented with protease inhibitor at 2 mg/ml final concentration, pH7.7). Pre-cleared lysates were incubated with the antibody-beads complex overnight at 4ºC. After washing twice with wash buffer (Tris-HCl 100 mM; NaCl 300 mM) supplemented with 1% (v/v) triton-X100 and twice with wash buffer without Triton, proteins were eluted in Laemmli buffer supplemented with 100mM DTT. Eluted proteins were allowed to load into a SDS-PAGE gel and run until reaching 1 cm into the separating gel. Silver nitrate staining was performed and the upper 1cm gel segment was preserved in PBS and used to MS analysis. All the analysis was performed in triplicate.

2.3. Mass spectrometry: sample preparation, analysis and dataset filtering

Eluted proteins were reduced with 10 mM of DTT for 40min at 56ºC followed by alkylation with 55mM iodoacetamide for 30min. The remaining iodoacetamide was quenched by a second incubation with 10mM DTT for 10min in the dark. Then, the resulting sample was digested overnight with trypsin at 37ºC (1:50 protein/trypsin ratio), dried and resuspended in 8µL LCMS water 0.1% formic acid.

NanoLC-MS/MS analysis was performed on an ekspert™ NanoLC 425 cHiPLC® system coupled with a TripleTOF® 6600 with a NanoSpray® III source (Sciex). Peptides were separated through reversed-phase chromatography (RP-LC) in a trap-and-elute mode. Trapping was performed at 2 µl/min with 100% A (0.1% formic acid in water, Fisher Chemicals, Geel, Belgium), for 10 min, on a Nano cHiPLC Trap column (Sciex 200 µm x 0.5 mm, ChromXP C18-CL, 3 µm, 120 Å). Separation was performed at 300 nl/min, on a Nano cHiPLC column (Sciex 75 µm x 15 cm, ChromXP C18-CL, 3 µm, 120 Å). The gradient was as follows: 0-1 min, 5% B (0.1% formic acid in acetonitrile, Fisher Chemicals); 1-91 min, 5-30% B; 91-93 min, 30-80% B; 93-108 min, 80% B; 108-110 min, 80-5% B; 110-127 min, 5% B. Peptides were sprayed into the MS through an uncoated fused-silica PicoTip™ emitter (360 µm O.D., 20 µm I.D., 10 ± 1.0 µm tip I.D., New Objective). The source parameters were set as follows: 12 GS1, 0 GS2, 30 CUR, 2.5 keV ISVF and 100 ºC IHT. An information dependent acquisition (IDA) method was set with a TOF-MS survey scan of 400-2000 m/z for 250 msec. The 50 most intense precursors were selected for subsequent fragmentation and the MS/MS were acquired in high sensitivity mode (150-1800 m/z for 40 msec each). The selection criteria for parent ions included a charge state between +2 and +5 and counts above a minimum threshold of 125 counts per second. Ions were excluded from further MSMS analysis for 12 s. Fragmentation was performed using rolling collision energy with a collision energy spread of 5.

The processing and analysis of the obtained mass spectra list were done using ProteinPilot™ software, with the Paragon search engine (version 5.0, Sciex). The following search parameters were set: search against Homo sapiens from Uniprot/SwissProt database (release 2015_05); Iodoacetamide, as Cys alkylation; Trypsin, as digestion; TripleTOF 6600, as the Instrument; ID focus as biological modifications and Amino acid substitutions; search effort as thorough; and a FDR analysis. Only the proteins with Unused Protein Score above 0.47 (corresponding to 66% confidence) were considered. This lower confidence threshold was selected to allow the detection of proteins that compensate their lower scores in single replicates by their identification in multiple replicates. If a protein is detected with 66% confidence in three replicates, the chance that all identifications were false positives is below 4% (below 11% for two replicates). To account for this effect, a Confidence score was developed, based on the unused ProtScore and the number of replicates in which each protein was detected (compared to controls). The range varies between 0 - protein identified with low robustness and confidence, and 5 - protein identified with high robustness and confidence as shown in Table S1. The proteins identified for parental CFBE41o- cells and for CFBE cells expressing wt-CFTR incubated with non-conjugated beads were considered as non-specific and removed from the protein lists identified for CFBE cells expressing wt-CFTR incubated with Fsk, 007-AM and DMSO. In this analysis, a protein is only excluded (appearing in controls) or considered (appearing in samples under analysis) as a specific protein when present in at least two replicates. To determine the score of each protein, the lists for each condition (CFBE cells incubated with DMSO, Fsk or 007-AM) were compared with the lists for the 2 controls used (parental cells and wt-CFTR cells incubated with beads only) to evaluate the associated Unused ProtScore and the number of replicates where the protein was identified in both samples and controls. R programming was used to calculate the Confidence score for each protein[1]. Lists of proteins identified in each of the three conditions tested were compared to identify common and specific proteins for each condition.

2.4. Networks and gene ontology

The Database for Annotation, Visualization and Integrated Discovery (DAVID)[2] [18,19] was used to analyze the obtained data set and identify the Gene Ontology (GO) terms which were enriched in our data. The GO terms considered were the Biologic process (BP) and Cellular Component (CC) using version 6.8.

Data were also analysed with Agile Protein Interactomes DataServer (APID) in combination with R programming [20]. APID human interactomes of quality level 0 (all reported interactions) or level 1 (interactions proven by 2 or more experimental evidences) were used to assess the distance (1 to 5 edges distance) of the identified proteins (proteins interacting with CFTR specifically after cell incubation with 007-AM) to proteins of interest (CFTR and EPAC1). APID level 0 was also used to generate protein networks. Finally, the shortest path in the network between two proteins of interest was determined using APID level 0 or APID level 1. Networks generated using APID [21] were accessed and visualized/analyzed using Cytoscape [22]. To generate the wt-CFTR general network, we used the proteins detected in our assays with a Confidence score of 2 or higher (Table S1) for all sample-control combinations, using APID level 0 as the basis for the PPI.

2.5. siRNA transfection

For siRNA transfection, cells were transfected 24h after being split. Transfection mixture using Lipofectamine 2000 (1 mg/ml, Invitrogen #11668019) was prepared containing 75nM of siRNA (CAPZA2 (Dharmacon #D-012213-17), INF2 (Dharmacon # D-014097-03), EGFP (Eurofins MWG operon #921154)) and 2.5 ng Lipofectamine to a final volume of 500 µL in OptiMEM, according to the manufacturer´s instructions. After transfection, cells were grown in

[1] R program, https://www.r-project.org/ (Last accessed March 09, 2019).
[2] DAVID database, https://david.ncifcrf.gov/ (Last accessed March 08, 2019)

FBS-free media. After 24h the media was changed to EMEM supplemented with 10% FBS (v/v). 48h after transfection, cells were harvested.

2.6. CFTR trafficking assay and image analysis

For cell reverse transfection, 96 well plates were coated with customized siRNAs for solid-phase reverse transfection. In short, a transfection mix (final volume of 300 µl) containing 161.5 µl of lipofectamine 2000 (Invitrogen #11668019) and 138.5 µl of 0.4 M sucrose in OptiMEM solution was prepared. Then, 1.25 µl siRNA 20 µM (Table S2 - Supplementary Data) were added to the respective well into the 96 v-shaped well plates (siRNA plate). 1.75 µl of transfection mix were added to siRNA plate, followed by mixing and centrifugation for 1 min at 50g. 1.75 µl of 0.2% (w/v) gelatin solution were added to the siRNA plate and centrifuged at 50g. A total of 4.25 µl of the siRNA plate mix (siRNA plus transfection mix plus gelatin) was diluted 1:50 in 96 v-shaped well plate using double distilled water. Finally, 50 µl from diluted mix were lyophilized and stored in an anhydrous atmosphere before cell seeding.
After 24h, cells were seeded in the siRNA coated 96-well plate (7 x 10^7 cells/well) using a Multidrop™ Combi Reagent Dispenser (Thermo Scientific #5840300). CFTR expression was induced after 24h of reverse transfection by incubating the cells with 1 µg/ml doxycycline in antibiotic-free medium. CFTR expression was induced for 24h.

72h after cell seeding and siRNA knockdown, cells were washed once with cold $PBS^{+/+}$ using Tecan Hydrospeed™ and immunostained for the extracellular FLAG-tag (in non-permeabilized cells) for 1h at 4ºC with 1:500 monoclonal anti-FLAG® M2 antibody (Sigma-Aldrich, #F1804). Then, cells were washed three times in ice with cold $PBS^{+/+}$ and incubated 20 min with 3% (w/v) paraformaldehyde (PFA) at 4ºC. Then, cells were then washed three times in ice with cold $PBS^{+/+}$ and incubated with the anti-mouse Cy5 conjugated secondary antibody (1:500) (Invitrogen, #A10524) for 1h at 4ºC. Cells were washed three times in cold $PBS^{+/+}$ and incubated for 1h with 1:5000 Hoechst 33342 solution (Sigma-Aldrich, #B2261) for nuclei staining. Finally, cells were washed three times in cold $PBS^{+/+}$ and immersed in $PBS^{+/+}$ until cell imaging. All solutions were prepared in $PBS^{+/+}$ and primary and secondary antibodies were diluted in $PBS^{+/+}$ supplemented with 1% (v/v) BSA.

For image acquisition, cell imaging was performed with inverted widefield fluorescence microscope Leica DMI6000 equipped with a DFC360FX camera (12-bit, 1344x1024 pixel resolution) (Leica) and a 10x objective. The exposure times at maximum light brightness for Hoechst, mCherry and Cy5 were 70ms, 1300ms and 8s respectively. The Hoechst channel was used for contrast-based autofocus. The experiment was performed in triplicate and five images were collected per well.

For image analysis, automatic image analysis was performed using open source software tools namely cell image analysis software CellProfiler[3] [23], R programing [20] and a pipeline to measure CFTR traffic efficiency developed previously [24]. Using the pipeline, the background was subtracted to each image. Then, a quality control was applied for each image excluding all cells which do not significantly express CFTR, present abnormal morphology or contain a significant number of saturated pixels. Out-of-focus images, images with high background fluorescence and images with lower number of cells (less than 15 cells) were also removed with this pipeline. Finally, CFTR levels were measured in each cell using the fluorescence quantification to determine Total CFTR, given by the mCherry fluorescence intensity and PM CFTR, given by Cy5 fluorescence intensity. CFTR traffic efficiency was calculated using the median values for all cells in the image and calculated according to the ratio PM CFTR (Cy5 Integrated Fluorescence) / TOTAL CFTR (mCherry Integrated Fluorescence). Then, the deviation score was calculated according to the following formula:

$$Deviation\ Score = \frac{Traffic\ Efficiency_{test} - Traffic\ Efficiency_{control}}{2 \times SEM_{control}}$$

[3] CellProfiler, http://cellprofiler.org/ (Last accessed February 21, 2019).

The Traffic Efficiency$_{Test}$ corresponds to the average of CFTR traffic efficiency for all images transfected with the same siRNAs or treated with the same compound which passed the QC. The Traffic Efficiency$_{control}$ corresponds to the average of CFTR traffic efficiency for all the conditions in the plate or in case of compound incubation the DMSO - All Conditions or DMSO. The standard error of the mean of the control (SEM$_{control}$) corresponds to the SEM recorded for the control condition - All Conditions or DMSO. Deviation score identifies traffic enhancers (when it is positive) or inhibitors (when it is negative).

2.7. Immunofluorescence assay

Cells were grown on glass coverslips and then washed three times on ice with cold PBS$^{+/+}$ for 5 min and fixed with 3% (w/v) paraformaldehyde for 15 min on ice. Cells were washed three times with cold PBS$^{+/+}$ and then permeabilized with 0.5% (v/v) Triton-X100 for 10min. After three washes with cold PBS+/+, cells were incubated for 1h with primary antibody- 1:50 mouse monoclonal anti-EPAC (A-5) (SantaCruz #sc-28366) or 1:50 rabbit polyclonal anti-INF2 (ProteinTech #20466-1AP) - at 4ºC and washed again three times with cold PBS$^{+/+}$. Then, cells were incubated for 1h with secondary antibody - 1:500 Alexafluor 488 IgG anti-rabbit (Invitrogen #A21206) or 1:500 Alexafluor 647 IgG anti-mouse (Invitrogen #A-31571) - followed by three washes with PBS$^{+/+}$. Cells were incubated with 1:5000 Hoechst 33342 (Sigma #B2261) for 15 min at 4ºC for nuclei staining. Finally, after three washes with cold PBS+/+, the coverslips were mounted in mounting solution (N-Propyl gallate 0.5%, 10xPBS 10%, Glycerol 90%) on glass slides and visualized by a Leica SP8 confocal microscope with a 63x objective. All solutions were prepared in PBS$^{+/+}$ and antibodies were diluted in PBS+/+ supplemented with 1%(w/v) BSA (Sigma-Aldrich, #A9647).

2.8. Cell-surface biotinylation assay

Cell surface biotnylation was performed as previously described [11,25]. Cells were grown in P60 plates until pre-confluence. After three washes with PBS^{++} cells were incubated at 4ºC with 3mL of Sulfo-NHS-SS-Biotin buffer (0.1mg biotin (Thermo Scientific, #21331)/1 mL PBS with 1mM MgCl2, 0.1mM CaCl2, pH 8.2) for 30 min and then washed three times with PBS^{++}. Cells were lysed with 1.5mL of BL buffer (HEPES 25mM, Triton X-100 1% (v/v), glycerol 10% (v/v), supplemented with complete protease inhibitor cocktail, pH 8.2) and incubated for 15min at 4ºC. Cell membranes and debris were pelleted by centrifugation at 14000g for 10min at 4ºC following by supernatant incubation at 4ºC overnight with streptavidin beads previously washed twice with PBS and once with BL buffer. The beads were pelleted by centrifugation 1min at maximum speed and next washed once with BL buffer and twice with PBS. Then, beads were incubated with 65µL SB suplemmented with DTT 1M at 85ºC for 5min. Finally, samples were loaded into a SDS-PAGE gel for western blotting analysis.

2.9. Western bloting

Protein extracts were separated on SDS polyacrylamide gel electrophoresis (PAGE) and transferred to PVDF membranes. Membranes were blocked and probed overnight with primary antibody at 4ºC (1:5000 mouse anti-CFTR 596 (CFF, Cat No A4), 1:1000 rabbit polyclonal RAPGEF3 antibody - middle region (Aviva Systems Biology, ARP52140_P050), 1:1000 rabbit polyclonal anti-CAPZA2 (ProteinTech, 15948-1-AP), 1:1000 rabbit polyclonal anti-INF2 (ProteinTech, 20466-1AP)). Calnexin, tubulin or GAPDH (1:3000 purified mouse anti-Calnexin (BD Transduction Laboratories™, 610523), 1:10000 mouse monoclonal anti-α-tubulin1 (Sigma, T5168), 1:1000 mouse monoclonal anti-GAPDH (6C5) (abcam, ab8245)) were detected as loading control. Membranes were washed three times followed by incubation for 1h with the adequate secondary antibody at room temperature (1:3000 goat anti-mouse IgG (H+L) HRP conjugate (Bio-Rad, 170-6516), 1:3000 goat anti-rabbit IgG (H+L) HRP conjugate (Bio-Rad, 170-6516)). Finally, membranes were washed three times with PBS-T. Antibody dilutions were all made in blocking solution (PBS-T plus 5% milk). Chemiluminescent detection was performed

using the Clarity™ Western ECL substrate (BioRad, #170-5061) and the Chemidoc™ XRS system (BioRad). The quantification of band intensity was performed using the Image Lab software (BioRad) and normalized to loading control as appropriate.

2.10. Statistical analysis

Data are presented as mean ± standard error of the mean (SEM). Two-tailed Student's t-tests were performed to quantify statistical significance. In these analyses, $p<0.05$ was considered as significant.

3. Results

3.1. Proteomic profiling of wt-CFTR through activation of EPAC1

In an attempt to identify the proteins involved in CFTR stabilization at the PM under EPAC1 activation, CFTR was immunoprecipitated from CFBE wt-CFTR cells under low-stringency conditions to maximize the number of interacting proteins obtained. As we were interested in identifying the differential interactors involved in CFTR stabilization by EPAC1, cells were incubated with: - forskolin (Fsk); - the specific EPAC1 agonist 007-AM (8-pCPT-2′-O-Me-cAMP) or - DMSO (vehicle control). Non-specific interactions ("background") were discarded using an equivalent approach in CFBE cells which do not express CFTR (parental CFBE cells) and in CFBE wt-CFTR cells incubated with non-conjugated beads. Isolated proteins were then identified using nanoLC-MS/MS.

We were able to pull-down a total of 1599 proteins (Table S3A - Supplementary Data). For CFBE cells expressing wt-CFTR incubated with DMSO, Fsk or 007-AM, a total of 311, 263 and 399 proteins were identified respectively (Table S3B - Supplementary Data). A total of 374 proteins were identified for CFBE parental cells and 251 proteins were identified for CFBE cells expressing wt-CFTR incubated with non-conjugated beads (Table S3B - Supplementary Data).

Removal of proteins identified in the controls resulted in a total of 207 different proteins (Table S4A - Supplementary Data) for the sum of the three conditions tested, that were then crossed to identify the specific proteins for each condition (Figure S1). CFTR is one of the three proteins that is common to all the conditions tested. Interestingly, the higher number of specific proteins was identified when EPAC1 is activated (CFBE cells incubated with 007-AM) – 101 proteins (Table S4B - Supplementary Data). In addition, 23 CFTR interacting proteins were identified specifically when adenylyl cyclase is activated (CFBE cells incubated with Fsk) and 62 CFTR interacting proteins were identified exclusively for the incubation with DMSO control condition (Figure S1; Table S4B - Supplementary Data).

3.2. Bioinformatic and comparative analysis of CFTR interacting proteins

We used available bioinformatics tools to analyse the lists of proteins interacting with wt-CFTR upon activation of either AC (incubation of cells with Fsk) or EPAC1 (Incubation of cells with 007-AM).

DAVID was used to identify the enriched GO terms among the 110 CFTR interacting proteins through EPAC1 activation (Figure 1). For GO term – BP, cellular component biogenesis, cellular component assembly and cell-cell adhesion are the most represented terms. There is also an overrepresentation of categories associated to the cytoskeleton and to actin filaments. For GO term – CC, adherent junction, anchoring junction and extracellular vesicle are the most represented terms. At the CC level, the increased representation of cytoskeleton and actin filaments-associated categories is even more evident since more than 2/3 of all categories represent cellular components which are strongly connected with cytoskeleton and actin filaments as shown in Figure 1B.

We then used APID to calculate the distance between the 110 proteins specifically identified after EPAC1 activation and either CFTR or EPAC1. The proteins were analysed with

APID level 0 (accounts for all known interactions) and APID level 1 (accounts for interactions proved by two or more experiments). In these 110 proteins, 6 proteins (based on both APID level 0 and APID level 1 – Figure S2A) were previously reported as interacting (directly) with CFTR (AHSA1, CSE1L, HSPA2, PPP2R1A, PSMD2 and NHERF1). Moreover, we found that more than 85% of the 110 proteins are within 2 to 3 edges of distance from CFTR (with the more stringent APID level 1). When measuring the distance of the 110 proteins to EPAC1, there was no protein detected previously reported in APID to interact directly with EPAC1 (Figure S2B). The fact that we pulled-down CFTR and not EPAC1 is a plausible explanation for this observation. However, more than 89% are within 3 to 4 edges of distance from EPAC1.

To analyse the robustness and confidence for the identified proteins, a scoring system (named Confidence score and detailed in Table S1) was developed. This Confidence score takes into consideration the Unused ProtScore and the number of replicates in which each protein was detected (comparing samples and controls). 5 proteins were identified with a high robustness and confidence (score – 5) for the interactors upon EPAC1 activation (Table S5 - Supplementary Data). CFTR is one of these proteins supporting the approach used as well as the reliability of the scoring methodology. For the proteins detected under EPAC1 activation, 27% were scored above or equal to 3.

Comparison with previously published interactomes [26][27] identified a very low overlap (around 2%) - suggesting that the 110 proteins correspond to proteins that specifically interact with CFTR when EPAC1 is activated and thus do not belong to the "core" CFTR interactome.

In order to select the hits for validation from the 110 interactors, all the data described above were integrated (Table S6 - Supplementary Data) and complemented with extensive literature-mining. We then selected for validation 3 proteins a Confidence score of 5, 7 proteins with a score of 4 and 3 proteins with a score of 3 (Table S6 - Supplementary Data). We also selected 5 proteins with a score of 2 (lower robustness and confidence) in order to evaluate the strength of the selection methodology used. Interestingly, from the 18 selected hits, 16 are within 2 edges of distance to CFTR and, from these 16 proteins, 15 are within 3 edges of distance to EPAC1 showing the high proximity of the selected hits to CFTR and EPAC1 (Table S6 - Supplementary Data).

3.3. Generation of protein networks

To assess the possible connections between the proteins identified, we generated a network using all proteins scored with 2 or higher in the Confidence score. For this, proteins identified in the controls were removed from the lists identified for each sample (Fsk, DMSO or 007-AM) resulting in a total of 260 proteins that were used for the network generation (Table S7 - Supplemmentary Data).

Using APID, we created a network exhibiting the association between the proteins identified based on previously reported interactions (Figure S3 - Supplemmentary Data). This large network shows that 201 proteins are connected. Moreover, the network shows that the proteins detected specifically after treatment with Fsk or DMSO (shown in green and blue respectively) as well as the proteins detected in more than one sample (shown in gray) are relevant in establishing the core of the network as they mediate the paths between the 110 proteins detected upon EPAC1 activation (shown in pink). CFTR, NHERF1 and EPAC1 (represented in yellow) appear as key components in this network, supporting the robustness (and relevance) of the results obtained. From the 251 proteins (interaction score ≥2), there are only 51 proteins that do not participate in previously described interactions. The general network obtained also shows that the 18 top hits selected for validation (shown with red border) are homogenously distributed rather than concentrated in a restricted area. This list of 18 selected proteins comprises proteins which are: 1) in close proximity to CFTR, with just one edge of distance; 2) distant from CFTR, with two or more edges of distance; 3) proteins creating small clusters among themselves and 4) proteins not present in the general network obtained.

As the 18 hits selected for validation seem to be in close proximity, we built a minimum network needed to link them to CFTR and EPAC1 (Figure 2) with APID level 1 as the source of interactions. This confirms that they can be linked through a minimal network to which only 8 additional proteins (shown in blue) are needed to connect them to CFTR and EPAC1 (shown in yellow) (Figure 2).

3.4. Impact of hit knockdown on CFTR trafficking

After selecting 18 hits for validation, we assessed the impact of their knockdown by siRNA upon CFTR trafficking using a previously described assay [24].

We started by validating the assay for the previously reported increase of CFTR trafficking upon EPAC1 activation (as reported by us in [11]). For that, we used CFBE cells expressing mCherry-Flag-wt-CFTR under the control of a doxycycline-inducible promoter, that were incubated with either the EPAC1 agonist 007-AM or DMSO (vehicle control). Immunostaining assay was performed and CFTR at the PM was monitored by the Flag (Cy5) signal. CFTR trafficking (given by the ratio of PM CFTR to total CFTR) and the deviation score were also calculated as described [24]. Results show that EPAC1 activation leads to an increase in wt-CFTR at the PM corresponding statistically significant increase in traffic efficiency (Figure 3). This result confirms this trafficking assay as robust to assess the impact of hit knockdown in combination with EPAC1 activation.

We assessed the impact of siRNA knockdown of the 18 selected hits upon wt-CFTR trafficking, comparing the 007-AM treatment with the vehicle control (DMSO). For this assay, cells were reverse transfected separately with 2 independent siRNA for each of the 18 selected genes for validation and siRNAs to CFTR, COPB1, EPAC1 and EGFP (non-targeting siRNA) were used as controls. 24h after transfection with siRNA, CFTR expression was induced. At 24h post-induction, immunofluorescence was performed. Total and PM for CFTR were assessed and the trafficking efficiency plotted (Figure 4). An effect on CFTR traffic efficiency was just considered when the two siRNAs targeting the same gene resulted in an equivalent effect.

Analysis of results (Figure 4C) shows that only the knockdown of INF2 (Inverted formin-2) has a major positive impact in the traffic efficiency of wt-CFTR (deviation score >1).

For INF2, both siRNAs lead to a significant increase in CFTR trafficking when combined with EPAC1 activation. This major positive impact of INF2 siRNA in the presence of 007-AM is also clearly observed in the representative images (Figure 4B-INF2_2).

With the opposite effect, CAPZA2 (Capping actin protein of muscle Z-line alpha subunit 2) was the only hit whose knockdown had a major negative impact in wt-CFTR traffic efficiency with both siRNAs showing a deviation score lower than -1 (for combination with EPAC1 treatment). CAPZA2 representative images clearly show the negative impact of the knockdown in the levels of wt-CFTR at the PM when cells were incubated with 007-AM (Figure 4A and B-CAPZA2_2). Thus, INF2 and CAPZA2 were selected to further investigate their impact in wt-CFTR PM levels. INF2 was scored with 4 in the Confidence score while CAPZA2 was scored with 3. Inverted formin-2 (INF2) is an unusual formin since it is the only formin with the ability to accelerate both actin polymerization and depolymerization controlling filament dynamics and regulating cell polarity, mitochondrial fission, intracellular trafficking as well as cell and tissue morphogenesis [28,29]. Capping actin protein of muscle Z-line alpha subunit 2 (CAPZA2) is a component of the heterodimeric actin-capping protein which binds to the fast growing ends of actin filaments (barbed end) blocking the exchange of subunits at these ends [30].

As to the other selected proteins, CALD1 and MYO1D were scored with 4 but their KD had no relevant impact in CFTR trafficking efficiency (Figure 4). Both siRNAs used against CALD1 showed a trend to decrease CFTR trafficking efficiency in the presence of 007-AM, however, the deviation score was > -1. The representative images show that CALD1 knockdown does not influence wt-CFTR levels at the PM (Figures 4A-CALD1_2 and 20B-CALD1_2). Knockdown of MYO1D had a null impact in wt-CFTR trafficking, despite its high Confidence score (Figure 4-MYO1D_2). TPM4 was scored with 2 and selected to evaluate the strength of the selection strategy used. CFTR trafficking assay showed that knockdown of this gene has no

impact in wt-CFTR trafficking to the PM (Figure 4-TPM4_2) as well as all the other proteins scored with 2 (FLG2, PSMB6, RPS14 and RPS18) supporting the selection strategy adopted. Being this a screening assay, we cannot of course exclude the fact that lack of an effect may correspond to low knock-down efficiency for the siRNA transfection.

3.5. Validation of INF2 and CAPZA2 as CFTR interactors under EPAC1 activation

As we aim to identify proteins involved in CFTR stabilization at the PM through EPAC1 activation, we then validated and characterized the role of the two hits identified: CAPZA2 and INF2. For that, we validated the interaction between CAPZA2 or INF2 proteins and CFTR and assessed the effect of knockdown of CAPZA2 and INF2 at 3 levels: *i)* the amount of wt-CFTR at the PM; ii) amount of EPAC1 interacting with CFTR and iii) cellular localization of CFTR and EPAC1 as compared to INF2 and CAPZA2. Interaction between EPAC1 and CAPZA2 or INF2 was also assessed to get additional information on its mechanism of action.

To validate the results obtained in the CFTR trafficking assay for CAPZA2 KD, we first assessed the efficiency of KD of both siRNA used against CAPZA2. Results show that both siCAPZA2 decrease the levels of protein by more than 50% as compared to siRNA against EGFP – the non-targeting siRNA (Figure S4B).

We then assessed the interaction between CAPZA2 and CFTR to validate the MS results. We performed the same pull-down used to prepare the samples for nanoLC-MS/MS. For that, CFTR was immunoprecipitated from CFBE wt-CFTR cells incubated with 007-AM or DMSO. Lysates incubated with beads only were used as a control. WB analysis shows that CAPZA2 is detected after CFTR IP when EPAC1 is activated (Figure 5A). The quantification of the interaction CFTR:CAPZA2 shows an increased interaction when cells were incubated with 007-AM (Figure 5B). The absence of CAPZA2 signal in cells incubated with DMSO and in the control confirms that CFTR:CAPZA2 interaction only occurs under EPAC1 activation.

For INF2, we also assessed first knockdown efficiency for both siRNAs (Figure S4C). Results show that both siRNAs against INF2 lead to a decrease in the levels of INF2 (40 to 60% reduction) as compared to the control (Figure S4D).

We started by validating the nanoLC-MS/MS results to confirm the CFTR:INF2 interaction. As after performing CFTR co-IP, we were not able to detect INF2 by WB, probably due to specific characteristics of the antibody, we used the reverse approach - detecting CFTR after immunoprecipitation of INF2. Results show that CFTR can be detected after INF2 immunoprecipitation in both cells treated with 007-AM or DMSO. However, the interaction is significantly increased after EPAC1 activation (Figure 5C and D). Moreover, our data suggest that INF2 presents a stronger affinity to the mature form of CFTR, as evidenced by a clear increase in Band C levels in Figure 5C. In conclusion, this result confirms INF2 as a stronger interactor of CFTR under EPAC1 activation.

3.6. CFTR levels at the PM after modulation of CAPZA2 and INF2

Results from the trafficking assay (Fig.4) indicate that INF2 and CAPZA2 influences CFTR trafficking to the PM with opposite effects. To confirm such observations, we assessed the impact of INF2 and CAPZA2 knockdown upon CFTR PM levels using cell surface biotinylation in CFBE wt-CFTR cells transfected with siRNAs against INF2 or CAPZA2 and incubated with 007-AM or DMSO.

Results show a statistically significant increase in the levels of PM CFTR after INF2 KD (Figure 6B) when compared to siRNA EGFP. Thus, our results indicate that INF2 knockdown further potentiates the increase of CFTR at the PM (Figure 6B) already described for EPAC1 activation [11].

On the other hand, for CAPZA2 knockdown, results show that it leads to a statistically significant decrease in CFTR PM levels (Figure 6B) comapred to siRNA EGFP.

So, cell surface biotinylation results further support the previous observations that INF2 and CAPZA2 influences the amount of CFTR at the P, with opposite effects.

3.7. Interaction between CAPZA2, INF2 and EPAC1

As INF2 and CAPZA2 apparently regulate CFTR PM levels upon EPAC1 activation, we then evaluate if these two proteins interact with EPAC1. Immunoprecipitation of EPAC1 was performed with a specific antibody from CFBE wt-CFTR cells (using DMSO or beads only as controls). Presence of INF2 and CAPZA2 was asssessed by WB.

We were able to detect CAPZA2 after EPAC1 IP mainly after 007-AM treatment (Figure 7A). Results show that the EPAC1:CAPZA2 interaction is increased by 2-fold when EPAC1 is activated (Figure 7B). Thus, our results indicate that CAPZA2 interacts with EPAC1 as well as with CFTR. For INF2, we were able to detect it after treatment with either 007-AM or DMSO, observing a slight increase (although not statistically significant) when cells are incubated with 007-AM (Figure 7A).

In conclusion, our results show a strong EPAC1:CAPZA2 interaction promoted by 007-AM and also an interaction between INF2 and EPAC1 (but in this case independent of EPAC1 activation). Thus, since we identified these novel interactions, we assessed the impact of CAPZA2 or INF2 knockdown in the EPAC1:CFTR reported interaction. For that, we used CFTR immunoprecipitation followed by detection of EPAC1. CFBE cells expressing wt-CFTR were transfected with siRNAs against INF2 or CAPZA2 and incubated with 007-AM. Results show that knockdown of either CAPZA2 or INF2 does not influence significantly the CFTR:EPAC1 interaction (Figure 5C and D). Thus, our results indicate that INF2 as well as CAPZA2 interacts with both CFTR and EPAC1 but their KD does not compromise the CFTR:EPAC1 interaction.

Since we validated interactions between the pairs CAPZA2:CFTR, CAPZA2:EPAC1 INF2:CFTR, INF2:EPAC1 and that both proteins regulate CFTR levels at the PM, the next step was to assess the cellular localization of INF2, EPAC1 and CFTR under incubation with 007-AM or DMSO and INF2 KD. In the presence of 007-AM, results show increased levels of both INF2 and CFTR in the PM vicinity when compared to DMSO treatment. It is also observed that incubation with 007-AM leads to an accumulation of EPAC1 close to the PM indicating that INF2, CFTR and EPAC1 are located at the same cellular compartment (Figure 8A).

Next, to understand the impact of INF2 knockdown in EPAC1 localization, cells were transfected with siRNA against INF2 or EGFP and then incubated with 007-AM or DMSO. Results show that INF2 knockdown leads to an increase in EPAC1 levels at the PM. These results suggest that INF2 plays a role in the regulation of EPAC1 cellular localization (Figure 8B). This accumulation of EPAC1 in the PM vicinity was even potentiated under treatment with 007-AM. CFTR levels at the PM are also increased on CFBE treatment with 007-AM and INF2 KD as described above (Figure 8B). In conclusion, immunofluorescence results show that INF2, CFTR and EPAC1 localize at the same cellular compartment under EPAC1 activation and that the expression levels of INF2 influences CFTR and EPAC1 localization.

4. Discussion

The net flow of CFTR activity depends on both the number of channels at the PM and the function of each individual channel. Whereas the latter is mainly mediated by cAMP-dependent activation of PKA that phosphorylates CFTR RD [13], CFTR levels at the PM depends on the amount that reaches the membrane and then on its stability at the surface – controlled by endocytosis and recycling machinery. Understanding the mechanisms through which CFTR PM levels are regulated is likely to identify targets amenable to modulation that can be used to design innovative therapeutic strategies. This is of particular interest as CFTR bearing F508del-CFTR can be rescued to the PM by different mechanisms however, the half-life of the rescued mutant protein is significantly reduced due to the high endocytosis rate or a reduction in recycling back to the PM [2,31].

Here, we aimed at better understanding the mechanism through which EPAC1 activation leads to CFTR stabilization at the PM by identifying the molecular complexes elicited during this process. Using co-immunoprecipitation of CFTR followed by mass spectrometry, we performed a comparative interactomics profiling of wt-CFTR under activation of adenylyl cyclase (treatment with Fsk) or EPAC1 (treatment with 007-AM). From the total of 1599 proteins identified, 110 were exclusively identified after EPAC1 activation (Figure S1). GO terms enrichment analysis (Figure 1) in this set of proteins identified a high representation of actin cytoskeleton associated categories. Whereas it is known that CFTR stability and function is strictly correlated with the actin cytoskeleton [32] and that EPAC1 activation is also involved in actin cytoskeleton organization [33], these results suggest that the previous described increase in CFTR and NHERF1 interaction [11] under Epac1 activation is related to the formation of macromolecular complexes that stabilize the connection of CFTR to the actin cytoskeleton.

From the 110 specific CFTR interacting proteins under EPAC1 activation, we selected 18 hits for validation based on the developed "Confidence score" (based on confidence levels and robustness of the MS data), the distance to CFTR and EPAC1 supported by extensive literature-mining.

To evaluate the relative proximity between CFTR, EPAC1 and the 18 selected hits, we then refined the network to create a minimal network needed to link the 18 selected proteins (Figure 2). Only 8 additional proteins (XPO1, RAP1A, EZR, CDK2, PPP1CB, PSMC4, ACTB and PAN2) were needed to connect the selection. Interestingly, EZR which is a well known CFTR and NHERF1 interactor [11,34] was one of these added proteins. Among the 18 hits, ACTB and XPO1 were previously described as CFTR interactors [35,36]. RAP1A was also added to build the minimal network – despite not being a direct CFTR interactor, it is regulated by the EPAC as cAMP induces the GEF activity of EPAC towards RAP1A [37].

To assess the impact of the selected proteins on CFTR trafficking to the PM, we used 2 siRNAs targeting each of the proteins and assessed CFTR traffic efficiency (calculated as the ratio of PM to Total CFTR). A major impact (|deviation score| > 1) was obtained under knockdown INF2 and CAPZA2 (Figure 4) while the remaining siRNAs showed only minor impact in CFTR traffic efficiency. INF2 KD showed a major positive impact (deviation score > 1) in CFTR trafficking efficiency to the PM when cells were incubated with 007-AM. A statistically significant increase was observed for both siRNAs suggesting that INF2 is involved in the process of CFTR trafficking to the PM and that its knockdown increased CFTR levels at the PM. CAPZA2 was the only protein that showed a statistically significant major negative impact (deviation score < -1) in CFTR trafficking to the PM when knocked down combined with EPAC1 activation. This result suggests that CAPZA2 plays a positive role in CFTR trafficking to the PM since its knockdown leads to a marked decrease in CFTR levels at the PM. In summary, the two proteins for which both siRNAs produced a significant effect are INF2 and CAPZA2 – both classified with high "Confidence score" (3 or higher) and located at 2 and 3 edge distance from CFTR as well as from EPAC1. To our knowledge, this is the first time that these two proteins are identified as CFTR interactors and that their silencing has an effect in CFTR trafficking. We proceeded with additional validation/characterization of these 2 hits.

CapZ proteins are heterodimeric proteins belonging to the capping proteins family which are actin-binding proteins [38]. CapZ proteins are highly conserved proteins from yeast to humans and are composed of two unrelated subunits α and β [39]. CapZ proteins plays a key role in Arp2/3 mediated actin polymerization, influencing several cellular processes such as cell migration and cell invasion [39]. They control actin dynamics by blocking the addition of actin monomers to the filament end thus effectively terminating its elongation [39,40]. CAPZA2 protein (CapZ subunit α2) has been associated with cancer aggressiveness [30]. CAPZA2 protein is regulated by different scaffold proteins, such as TNKS1BP1, whose depletion causes a decrease in the association between CAPZA2 and actin filaments.

Our results show that CAPZA2 interacts specifically with wt-CFTR and its KD decreases CFTR leading to a reduced efficiency in CFTR trafficking to the PM under EPAC1 activation. We validated these observations using CFTR immunoprecipitation followed by detection of CAPZA2, confirming that the interaction is detected only upon EPAC1 activation (Figure 5A), and also cell surface biotinylation showing that CAPZA2 knockdown in combination with the

activation of EPAC1 pathway (promoted by incubation with 007-AM) leads to a statistically significant decrease in wt-CFTR at the PM compared to the non-targeting siEGFP (Figure 6). This association has not been previously described and suggests a role for CAPZA2 in regulating wt-CFTR at the cell surface. It was reported that CFTR anchoring to the actin filaments is associated to the activation of the small GTPase Rac1 through PIP5K and Arp2/3 such that Arp3 knockdown drastically impairs retention of CFTR at the PM [41]. Arp2/3 complex acts as an actin nucleator playing a key role in actin dynamics [42]. In the presence of capping proteins, branching by Arp2/3 complex is favoured, whereas capping protein depletion leads to a formation of actin bundles and thus, affecting cell shape [42,43].

The wt-CFTR:CAPZA2 association under EPAC1 activation is observed simultaneously with an increased interaction between EPAC1 and CAPZA2 (Figure 7A). Interestingly, CAPZA2 knockdown does not influence the interaction EPAC1:CFTR (Figure 7C). It is known that under EPAC1 activation, CFTR interacts directly with NHERF1 which then interacts with EPAC1 and ezrin. NHERF1:ezrin interaction locks CFTR in an immobile and actin-tethered complex preventing its endocytosis [8,9,11]. Thus, the increased EPAC1:CAPZA2 interaction verified under EPAC1 activation (Figure 7A) indicates that CAPZA2 further potentiate the CFTR anchoring at the PM. However, the fact that CAPZA2 KD does not influence CFTR:EPAC1 interaction (Figure 7C) may indicate that the presence of CAPZA2 plays an additive effect on CFTR anchoring at the PM and it is not a key element for the maintenance of the complex since it KD does not disrupt the complex. Thus, we suggest that CAPZA2 promotes the anchoring of wt-CFTR at the PM by stabilizing actin cytoskeleton which consequently leads to a stabilization of the CFTR-NHERF1-Ezrin-EPAC1 complex.

INF2 belongs to the formins family which are actin assembly factors that regulate a wide variety of actin-based structures, including stress fibers and actin filaments [44]. [44–46]. INF2 is unique among the formins due to its ability to accelerate depolymerization, in addition to the nucleation and elongation activity characteristic of the common formins. INF2 has been described as playing a key role in vesicular trafficking, mitochondrial dynamics, microtubule stabilization and centrosome orientation [29,44].

Our results show that CFTR interacts with INF2, an association that is increased upon EPAC1 activation and that involves mainly the mature form of CFTR (Band C) (Figure 5C). Such association suggests that INF2 may participate in CFTR trafficking and/or stabilization at the PM. The effect observed in the trafficking assay was confirmed using cell surface biotinylation with INF2 knockdown (in the presence of 007-AM) promoting a statistically significant increase in wt-CFTR at the PM as compared to the control (Figure 6).

As mentioned above, INF2 is the unique formin with the ability to accelerate actin nucleation and elongation (common formins ability) as well as to sever actin filaments and accelerate their depolymerization [47]. Biochemically, the FH2 domain of INF2 can accelerate significantly the actin nucleation regulating elongation by remaining processively bound to the fast-growing barbed end of the actin filaments. The FH1 domain binds the actin monomer-binding protein profilin, accelerating the elongation rate of the FH2-bound barbed end [29,48]. INF2 depolymerization activity is dependent on its unique C-terminus which contains an actin-binding WASP homology 2 (WH2) motif that sequester actin monomers in 1:1 complexes. INF2 C-terminus is also required for fast filament severing [44]. INF2-mediated depolymerization and severing are phosphate-dependent such that both processes are a consequence of phosphate release from the filament. INF2 severing ability is directly associated with the increased rate of actin filaments depolymerization since it increases the number of depolymerizable ends [44]. This occurs as the FH2 domain of INF2 inhibits the barbed end capping by capping proteins [44].

This triphasic function suggests that the role of INF2 expression may depend on the context/environment. Chen and collaborators described that INF2 overexpression induces formation of actin stress fibers which is closely associated with cell death. A different report shows that exposure to H_2O_2 increases INF2 expression which induces mitochondrial stress and consequently may lead to cell death [49]. Heuser and collaborators showed that INF2 is frequently overexpressed in basal-like breast cancer cell lines playing a role in cell migration, invasion and proliferation [50].

To further understand the mechanism through which INF2 impacts on CFTR PM stability under EPAC1 activation, we determined that EPAC1 and INF2 also interact (Figure 7A) but that, as described above for CAPZA2, INF2 knockdown does not affect the amount of EPAC1 which interacts with CFTR (Figure 7C). These results suggest that INF2 is involved in CFTR anchoring at the PM however, it is not a key element in CFTR-EPAC1 complex maintenance. Thus, we suggest that INF2 hampers the anchoring of wt-CFTR at the PM by improving actin cytoskeleton dynamics which interfere with stabilization of the CFTR-EPAC1 complex.

INF2 is localized mainly to the cytoplasm where it is peripherally bound to the cytoplasmic face of the ER and at the perinuclear rim [51,52]. We assessed the localization of INF2, CFTR and EPAC1 in CFBE cells by immunofluorescence. We show that there is an accumulation of INF2 at the PM showing that both CFTR and INF2 localize at the same cellular compartment in the case of EPAC1 activation (Figure 8). This result corroborates the previous observation that INF2:CFTR interaction is stimulated by the activation of EPAC1. INF2 knockdown combined with EPAC1 activation led to an increase in PM wt-CFTR (Figure 8B). Thus, this finding confirms the previous results showing that INF2 knockdown increases the levels of PM CFTR (results from the cell surface biotinylation) and increases CFTR trafficking efficiency (results from CFTR trafficking assays).

It was described previously that INF2 may bind to different regions of the actin filaments, namely: i) to the barbed ends; ii) near to the barbed ends; and iii) at the pointed ends controlling actin cytoskeleton dynamics [44,47]. The site where INF2 binds to the filament may influence its impact in the regulation of the filament dynamics, with roles in polymerization, severing or depolymerization – being its role determined by the levels of actin, INF2 and profilin inside the cell [47,49].

Our results, namely the INF2 localization studies showing that in wt-CFBE cells it localizes in the PM vicinity close to CFTR and EPAC1, under EPAC1 activation, suggest that the impact of INF2 in CFTR regulation is associated with polymerization events at the barbed ends of the filaments or with INF2-mediated severing near to the barbed ends. In both cases, INF2 activity affects actin cytoskeleton dynamics which may explain the positive impact of INF2 KD observed in wt-CFBE cells under EPAC1 activation (Figure 8B). We also showed that EPAC1 activation increases the levels of INF2, CFTR and EPAC1 at the PM vicinity with the 3 proteins localizing at the same compartment (Figure 8). This result further supports our hypothesis that INF2 interacts with both CFTR and EPAC1. Results also show that INF2 knockdown promotes the accumulation of EPAC1 at the PM - this effect is increased under EPAC1 activation suggesting a role for INF2 in regulating EPAC1 localization.

We proposed that CAPZA2 stabilizes the barbed end of actin filaments promoting wt-CFTR anchoring at the PM. On the other hand, our results suggest that INF2 regulates CFTR anchoring at the PM through polymerization events at the barbed ends of the filaments or with INF2-mediated severing near to the barbed ends. Thus, considering our results and the fact that CAPZA2 and INF2 were simultaneously identified as CFTR interactors under EPAC1 activation, we may hypothesize a combined effect for the two proteins. So, altogether our data suggest that while CAPZA2 stabilizes the barbed ends of actin filaments, INF2 binds laterally near to the barbed ends of the the actin filaments promoting its severing. With an opposite effect, INF2 and CAPZA2 together promote a balanced effect on the regulation of actin cytoskeleton dynamics and thus of CFTR PM stability.

Despite the combined model proposed for CAPZA2/INF2 regulation of CFTR anchoring at the PM, a competitive model cannot be excluded. Interestingly, several studies report a competition between formins and capping proteins for the actin filaments barbed ends **[53–55]**. In fission yeast, cytokinesis formin Cdc12p competes with capping protein for the actin barbed end through a profilin mediated process **[54]**. In human podocytes, INF2 interacts with profilin 2 and with the F-actin capping protein CAPZA1 playing a critical role in the tight regulation of actin and microtubule dynamics **[55]**. Such reports suggest that the opposite effects of CAPZA2 and INF2 in regulating CFTR PM levels under EPAC1 activation may also be explained by a competition or at least a contrasting role in binding actin filaments barbed ends in bronchial epithelial cells.

5. Conclusions

We identified 2 novel CFTR interactors which are involved in CFTR trafficking and anchoring to the PM. Based on our results, we propose that, as a capping protein, CAPZA2 binds to the barbed end of actin filaments blocking the uncontrolled addition of actin monomers to the filaments and consequently terminating the elongation. Without disturbing the actin cytoskeleton, CAPZA2 forms a complex with CFTR and EPAC1 at the end of actin filaments, thus in the vicinity of the PM promoting CFTR stabilization at the PM. In the absence of CAPZA2 the nucleation and depolymerization processes occurs in an uncontrolled manner leading to a decrease in wt-CFTR at the PM.

Additionally, we showed that INF2 plays an important role in CFTR trafficking to the PM since INF2 knockdown increases PM CFTR. EPAC1:INF2 interaction was also observed. However, despite not influencing CFTR:EPAC1 interaction, INF2 knockdown highly influences EPAC1 localization in CFBE cells. Thus, our results indicate that INF2 binds to actin filament barbed ends or side-bound close to the barbed ends controlling actin cytoskeleton dynamics interfering negatively with CFTR anchoring at the PM.

We hypothesize a combined/competitive effect for these two proteins where CAPZA2 stabilizes the barbed ends of actin filaments and INF2 binds laterally near to the barbed ends of the actin filaments promoting its severing. Thus, with an opposite effect, we suggest that INF2 and CAPZA2 together promote a balanced effect on the regulation of actin cytoskeleton dynamics and thus of CFTR PM stability.

In general these results confirm the role of the cytoskeleton-related interactions in regulating CFTR PM levels and stability and identify such processes as relevant for the increase of PM CFTR after an increase of cAMP and concomitant activation of EPAC1.

Acknowledgments

Work supported by centre grant UID/MULTI/04046/2019 to BioISI. J.D.S was recipient of PD/BD/106084/2015 PhD fellowship (FCT, Portugal).

Author contributions statement

J.D.S designed and performed the experiments, analysed data and wrote the paper; F.R.P. guided the experiments design for bioinformatic analysis and provided advice; M.D.A and M.Z. provided advice and comments on paper; C.M.F guided the project, guided the experiments design and reviewed the manuscript.

References

[1] F.S. Collins, Cystic fibrosis: molecular biology and therapeutic implications, Science, 256 (1992) 774–779.

[2] C.M. Farinha, J. King-Underwood, M. Sousa, A.R. Correia, B.J. Henriques, M. Roxo-Rosa, A.C. Da Paula, J. Williams, S. Hirst, C.M. Gomes, M.D. Amaral, Revertants, low temperature, and correctors reveal the mechanism of F508del-CFTR rescue by VX-809 and suggest multiple agents for full correction, Chem. Biol., 20 (2013) 943–955.

[3] J.R. Riordan, CFTR Function and Prospects for Therapy, Annual Review of Biochemistry, 77 (2008) 701–726.

[4] J.M. Rommens, M.C. Iannuzzi, B. Kerem, M.L. Drumm, G. Melmer, M. Dean, R. Rozmahel, J.L. Cole, D. Kennedy, N. Hidaka, Identification of the cystic fibrosis gene: chromosome walking and jumping, Science, 245 (1989) 1059–1065.

[5] C.M. Farinha, S. Canato, From the endoplasmic reticulum to the plasma membrane: mechanisms of CFTR folding and trafficking, Cell. Mol. Life Sci., 74 (2017) 39–55.

[6] T. Okiyoneda, H. Barrière, M. Bagdány, W.M. Rabeh, K. Du, J. Höhfeld, J.C. Young, G.L. Lukacs, Peripheral protein quality control removes unfolded CFTR from the plasma membrane, Science, 329 (2010) 805–810.

[7] P.M. Haggie, J.K. Kim, G.L. Lukacs, A.S. Verkman, Tracking of Quantum Dot-labeled CFTR Shows Near Immobilization by C-Terminal PDZ Interactions, Mol Biol Cell, 17 (2006) 4937–4945.

[8] C.M. Farinha, P. Matos, M.D. Amaral, Control of cystic fibrosis transmembrane conductance regulator membrane trafficking: not just from the endoplasmic reticulum to the Golgi, FEBS J., 280 (2013) 4396–4406.

[9] W.B. Guggino, B.A. Stanton, New insights into cystic fibrosis: molecular switches that regulate CFTR, Nat. Rev. Mol. Cell Biol., 7 (2006) 426–436.

[10] S.-H. Kwon, H. Pollard, W.B. Guggino, Knockdown of NHERF1 enhances degradation of temperature rescued DeltaF508 CFTR from the cell surface of human airway cells, Cell. Physiol. Biochem., 20 (2007) 763–772.

[11] M.J. Lobo, M.D. Amaral, M. Zaccolo, C.M. Farinha, EPAC1 activation by cAMP stabilizes CFTR at the membrane by promoting its interaction with NHERF1, J Cell Sci, (2016) jcs.185629.

[12] J. de Rooij, H. Rehmann, M. van Triest, R.H. Cool, A. Wittinghofer, J.L. Bos, Mechanism of regulation of the Epac family of cAMP-dependent RapGEFs, J. Biol. Chem., 275 (2000) 20829–20836.

[13] S. Monterisi, M. Favia, L. Guerra, R.A. Cardone, D. Marzulli, S.J. Reshkin, V. Casavola, M. Zaccolo, CFTR regulation in human airway epithelial cells requires integrity of the actin cytoskeleton and compartmentalized cAMP and PKA activity, J Cell Sci, 125 (2012) 1106–1117.

[14] C. Ulucan, X. Wang, E. Baljinnyam, Y. Bai, S. Okumura, M. Sato, S. Minamisawa, S. Hirotani, Y. Ishikawa, Developmental changes in gene expression of Epac and its upregulation in myocardial hypertrophy, American Journal of Physiology-Heart and Circulatory Physiology, 293 (2007) H1662–H1672.

[15] M. Schmidt, F.J. Dekker, H. Maarsingh, Exchange protein directly activated by cAMP (epac): a multidomain cAMP mediator in the regulation of diverse biological functions, Pharmacol. Rev., 65 (2013) 670–709.

[16] J. Lérias, M. Pinto, R. Benedetto, R. Schreiber, M. Amaral, M. Aureli, K. Kunzelmann, Compartmentalized crosstalk of CFTR and TMEM16A (ANO1) through EPAC1 and ADCY1, Cellular Signalling, 44 (2018) 10–19.

[17] K.M. Hoque, O.M. Woodward, D.B. van Rossum, N.C. Zachos, L. Chen, G.P.H. Leung, W.B. Guggino, S.E. Guggino, C.-M. Tse, Epac1 mediates protein kinase A-independent mechanism of forskolin-activated intestinal chloride secretion, J. Gen. Physiol., 135 (2010) 43–58.

[18] D.W. Huang, B.T. Sherman, R.A. Lempicki, Systematic and integrative analysis of large gene lists using DAVID bioinformatics resources, Nat Protoc, 4 (2009) 44–57.

[19] D.W. Huang, B.T. Sherman, R.A. Lempicki, Bioinformatics enrichment tools: paths toward the comprehensive functional analysis of large gene lists, Nucleic Acids Res., 37 (2009) 1–13.
[20] R. Core Team, R: A Language and Environment for Statistical Computing, (2018).
[21] D. Alonso-López, M.A. Gutiérrez, K.P. Lopes, C. Prieto, R. Santamaría, J. De Las Rivas, APID interactomes: providing proteome-based interactomes with controlled quality for multiple species and derived networks, Nucleic Acids Res., 44 (2016) W529–535.
[22] P. Shannon, A. Markiel, O. Ozier, N.S. Baliga, J.T. Wang, D. Ramage, N. Amin, B. Schwikowski, T. Ideker, Cytoscape: a software environment for integrated models of biomolecular interaction networks, Genome Res., 13 (2003) 2498–2504.
[23] A.E. Carpenter, T.R. Jones, M.R. Lamprecht, C. Clarke, I.H. Kang, O. Friman, D.A. Guertin, J.H. Chang, R.A. Lindquist, J. Moffat, P. Golland, D.M. Sabatini, CellProfiler: image analysis software for identifying and quantifying cell phenotypes, Genome Biol., 7 (2006) R100.
[24] H.M. Botelho, I. Uliyakina, N.T. Awatade, M.C. Proença, C. Tischer, L. Sirianant, K. Kunzelmann, R. Pepperkok, M.D. Amaral, Protein traffic disorders: an effective high-throughput fluorescence microscopy pipeline for drug discovery, Sci Rep, 5 (2015) 9038.
[25] S. Luz, K.M. Cihil, D.L. Brautigan, M.D. Amaral, C.M. Farinha, A. Swiatecka-Urban, LMTK2-mediated phosphorylation regulates CFTR endocytosis in human airway epithelial cells, J. Biol. Chem., 289 (2014) 15080–15093.
[26] D.M. Hutt, S. Loguercio, A.R. Campos, W.E. Balch, A Proteomic Variant Approach (ProVarA) for Personalized Medicine of Inherited and Somatic Disease, J. Mol. Biol., 430 (2018) 2951–2973.
[27] S. Pankow, C. Bamberger, D. Calzolari, S. Martínez-Bartolomé, M. Lavallée-Adam, W.E. Balch, J.R. Yates, ΔF508 CFTR interactome remodelling promotes rescue of cystic fibrosis, Nature, 528 (2015) 510–516.
[28] K.Y.B. Lamm, M.L. Johnson, J. Baker Phillips, M.B. Muntifering, J.M. James, H.N. Jones, R.W. Redline, A. Rokas, L.J. Muglia, Inverted formin 2 regulates intracellular trafficking, placentation, and pregnancy outcome, Elife, 7 (2018).
[29] V. Ramabhadran, A.L. Hatch, H.N. Higgs, Actin monomers activate inverted formin 2 by competing with its autoinhibitory interaction, J. Biol. Chem., 288 (2013) 26847–26855.
[30] E.A. Barron-Casella, M.A. Torres, S.W. Scherer, H.H.Q. Heng, L.-C. Tsui, J.F. Casella, Sequence Analysis and Chromosomal Localization of Human Cap Z CONSERVED RESIDUES WITHIN THE ACTIN-BINDING DOMAIN MAY LINK CAP Z TO GELSOLIN/SEVERIN AND PROFILIN PROTEIN FAMILIES, J. Biol. Chem., 270 (1995) 21472–21479.
[31] A. Swiatecka-Urban, A. Brown, S. Moreau-Marquis, J. Renuka, B. Coutermarsh, R. Barnaby, K.H. Karlson, T.R. Flotte, M. Fukuda, G.M. Langford, B.A. Stanton, The short apical membrane half-life of rescued {Delta}F508-cystic fibrosis transmembrane conductance regulator (CFTR) results from accelerated endocytosis of {Delta}F508-CFTR in polarized human airway epithelial cells, J. Biol. Chem., 280 (2005) 36762–36772.
[32] S. Castellani, M. Favia, L. Guerra, A. Carbone, A.C. Abbattiscianni, S. Di Gioia, V. Casavola, M. Conese, Emerging relationship between CFTR, actin and tight junction organization in cystic fibrosis airway epithelium, Histol. Histopathol., 32 (2017) 445–459.
[33] Kato Yuko, Yokoyama Utako, Yanai Chiharu, Ishige Rina, Kurotaki Daisuke, Umemura Masanari, Fujita Takayuki, Kubota Tetsuo, Okumura Satoshi, Sata Masataka, Tamura Tomohiko, Ishikawa Yoshihiro, Epac1 Deficiency Attenuated Vascular Smooth Muscle Cell Migration and Neointimal Formation, Arteriosclerosis, Thrombosis, and Vascular Biology, 35 (2015) 2617–2625.
[34] J. Li, Z. Dai, D. Jana, D.J.E. Callaway, Z. Bu, Ezrin controls the macromolecular complexes formed between an adapter protein Na+/H+ exchanger regulatory factor and the cystic fibrosis transmembrane conductance regulator, J. Biol. Chem., 280 (2005) 37634–37643.
[35] J. Colas, G. Faure, E. Saussereau, S. Trudel, W.M. Rabeh, S. Bitam, I.C. Guerrera, J. Fritsch, I. Sermet-Gaudelus, N. Davezac, F. Brouillard, G.L. Lukacs, H. Herrmann, M. Ollero, A.

Edelman, Disruption of cytokeratin-8 interaction with F508del-CFTR corrects its functional defect, Hum Mol Genet, 21 (2012) 623–634.
[36] X. Wang, J. Venable, P. LaPointe, D.M. Hutt, A.V. Koulov, J. Coppinger, C. Gurkan, W. Kellner, J. Matteson, H. Plutner, J.R. Riordan, J.W. Kelly, J.R. Yates, W.E. Balch, Hsp90 cochaperone Aha1 downregulation rescues misfolding of CFTR in cystic fibrosis, Cell, 127 (2006) 803–815.
[37] J. de Rooij, F.J. Zwartkruis, M.H. Verheijen, R.H. Cool, S.M. Nijman, A. Wittinghofer, J.L. Bos, Epac is a Rap1 guanine-nucleotide-exchange factor directly activated by cyclic AMP, Nature, 396 (1998) 474–477.
[38] C. Hug, T.M. Miller, M.A. Torres, J.F. Casella, J.A. Cooper, Identification and characterization of an actin-binding site of CapZ, J. Cell Biol., 116 (1992) 923–931.
[39] Y.-J. Jo, W.-I. Jang, S. Namgoong, N.-H. Kim, Actin-capping proteins play essential roles in the asymmetric division of maturing mouse oocytes, J. Cell. Sci., 128 (2015) 160–170.
[40] J.E. Caldwell, S.G. Heiss, V. Mermall, J.A. Cooper, Effects of CapZ, an actin capping protein of muscle, on the polymerization of actin, Biochemistry, 28 (1989) 8506–8514.
[41] S. Moniz, M. Sousa, B.J. Moraes, A.I. Mendes, M. Palma, C. Barreto, J.I. Fragata, M.D. Amaral, P. Matos, HGF stimulation of Rac1 signaling enhances pharmacological correction of the most prevalent cystic fibrosis mutant F508del-CFTR, ACS Chem. Biol., 8 (2013) 432–442.
[42] L.M. McMillen, D. Vavylonis, Model of turnover kinetics in the lamellipodium: implications of slow- and fast- diffusing capping protein and Arp2/3 complex, Phys Biol, 13 (2016) 066009.
[43] K. Dürre, F.C. Keber, P. Bleicher, F. Brauns, C.J. Cyron, J. Faix, A.R. Bausch, Capping protein-controlled actin polymerization shapes lipid membranes, Nat Commun, 9 (2018) 1630.
[44] E.S. Chhabra, H.N. Higgs, INF2 Is a WASP Homology 2 Motif-containing Formin That Severs Actin Filaments and Accelerates Both Polymerization and Depolymerization, J. Biol. Chem., 281 (2006) 26754–26767.
[45] D.R. Kovar, E.S. Harris, R. Mahaffy, H.N. Higgs, T.D. Pollard, Control of the assembly of ATP- and ADP-actin by formins and profilin, Cell, 124 (2006) 423–435.
[46] D. Vavylonis, D.R. Kovar, B. O'Shaughnessy, T.D. Pollard, Model of formin-associated actin filament elongation, Mol. Cell, 21 (2006) 455–466.
[47] P.S. Gurel, M. A, B. Guo, R. Shu, D.F. Mierke, H.N. Higgs, Assembly and turnover of short actin filaments by the formin INF2 and profilin, J. Biol. Chem., 290 (2015) 22494–22506.
[48] A.S. Paul, T.D. Pollard, Review of the mechanism of processive actin filament elongation by formins, Cell Motil. Cytoskeleton, 66 (2009) 606–617.
[49] Z. Chen, C. Wang, N. Yu, L. Si, L. Zhu, A. Zeng, Z. Liu, X. Wang, INF2 regulates oxidative stress-induced apoptosis in epidermal HaCaT cells by modulating the HIF1 signaling pathway, Biomedicine & Pharmacotherapy, 111 (2019) 151–161.
[50] V.D. Heuser, N. Mansuri, J. Mogg, S. Kurki, H. Repo, P. Kronqvist, O. Carpén, M. Gardberg, Formin Proteins FHOD1 and INF2 in Triple-Negative Breast Cancer: Association With Basal Markers and Functional Activities, Breast Cancer (Auckl), 12 (2018).
[51] E.S. Chhabra, V. Ramabhadran, S.A. Gerber, H.N. Higgs, INF2 is an endoplasmic reticulum-associated formin protein, J Cell Sci, 122 (2009) 1430–1440.
[52] X. Shao, K. Kawauchi, G.V. Shivashankar, A.D. Bershadsky, Novel localization of formin mDia2: importin β-mediated delivery to and retention at the cytoplasmic side of the nuclear envelope, Biol Open, 4 (2015) 1569–1575.
[53] E.S. Harris, F. Li, H.N. Higgs, The mouse formin, FRLalpha, slows actin filament barbed end elongation, competes with capping protein, accelerates polymerization from monomers, and severs filaments, J. Biol. Chem., 279 (2004) 20076–20087.
[54] D.R. Kovar, J.-Q. Wu, T.D. Pollard, Profilin-mediated Competition between Capping Protein and Formin Cdc12p during Cytokinesis in Fission Yeast, Mol Biol Cell, 16 (2005) 2313–2324.

[55] R. Rollason, M. Wherlock, J.A. Heath, K.J. Heesom, M.A. Saleem, G.I. Welsh, Disease causing mutations in inverted formin 2 regulate its binding to G-actin, F-actin capping protein (CapZ α-1) and profilin 2, Biosci. Rep., 36 (2016) e00302.

Figures

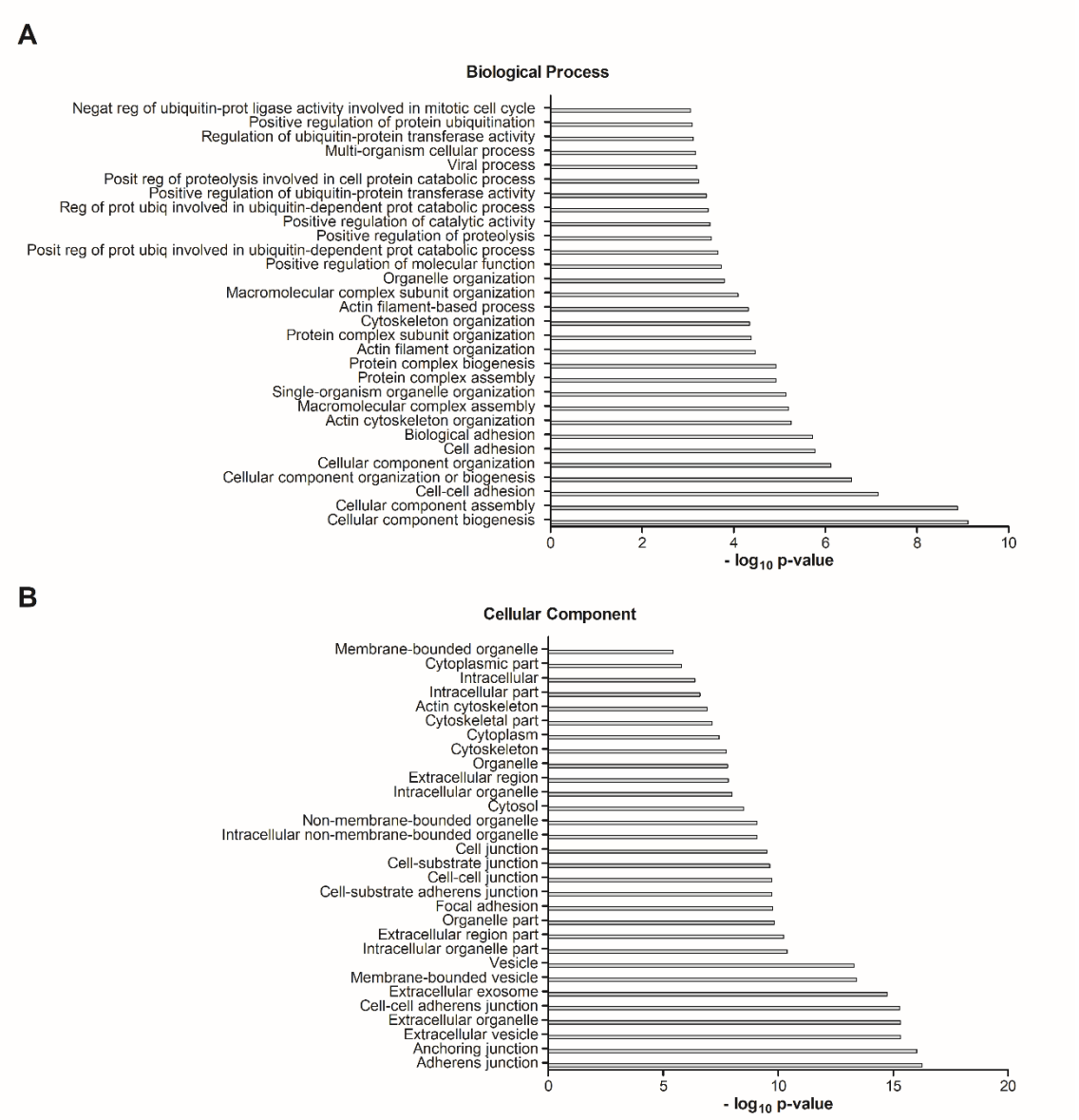

Figure 1: Analysis of GO terms for the specific CFTR interacting proteins under EPAC1 activation using DAVID. From the total of 1599 proteins, 110 specific CFTR interacting proteins under EPAC1 activation were used to find the Go Terms: **A)** Biological process and **B)** Cellular component.

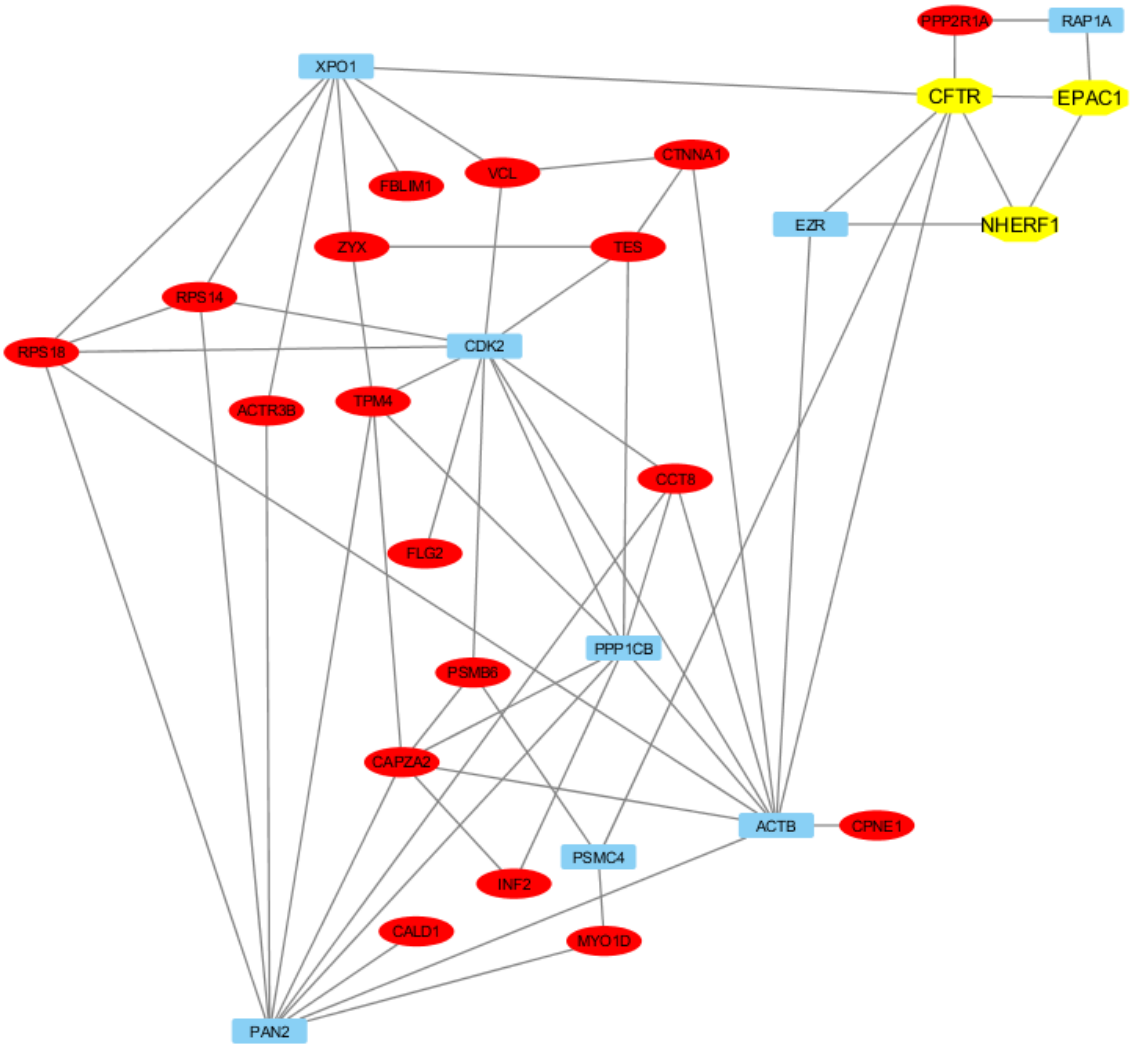

Figure 2: Minimal network needed to connect the 18 selected hits to CFTR, NHERF1 and EPAC1. RAP1A, XPO1, EZR, CDK2, PPP1CB, PSMC4, ACTB and PAN2 (represented in blue) are the 8 proteins needed to link the 18 selected hits for validation (represented in red) to CFTR, EPAC1 and NHERF1 (represented in yellow). R programming was used to calculate the shortest path between all the 18 proteins to CFTR, EPAC1 and NHERF1. Cytoscape platform was used to visualize the network using APID1 PPIs as the background.

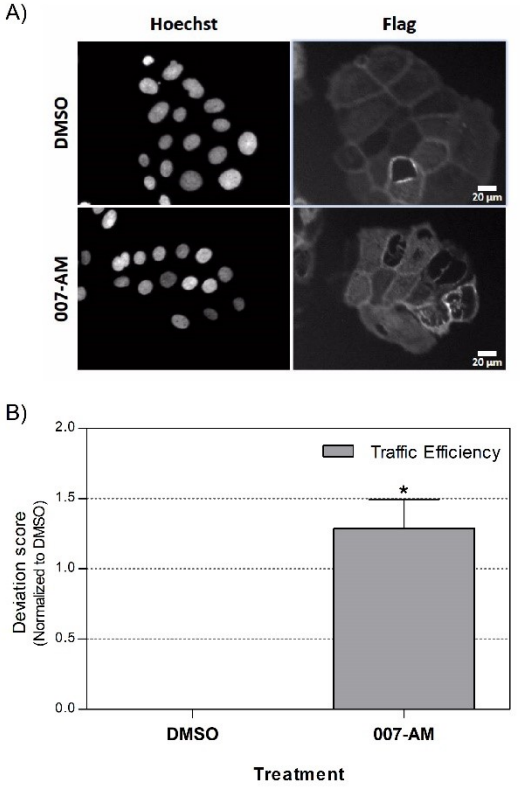

Figure 3: EPAC1 agonist (007-AM) increases CFTR trafficking to the PM. CFBE cells expressing mCherry-Flag-wt-CFTR under the control of a doxycycline-inducible promotor were incubated with 007-AM (1µM, 2h) or DMSO as a control. Immunostaining assay was performed and nuclei were stained with Hoechst 33342. Cy5 (immuno)fluorescence is proportional to the amount of Flag exposed extracellularly (CFTR present at the PM). **A)** Representative images obtained after immunostaining assay. CFBE cells expressing mCherry-Flag-wt-CFTR under an inducible promoter incubated with 007-AM (1µM, 2h) or vehicle control; **B)** Quantification of mCherry-Flag-wt-CFTR fluorescence relatively to the DMSO. Data are shown as the median deviation to DMSO, n=3. * $p<0.05$. Statistical analysis was performed using two-tailed unpaired students t-test.

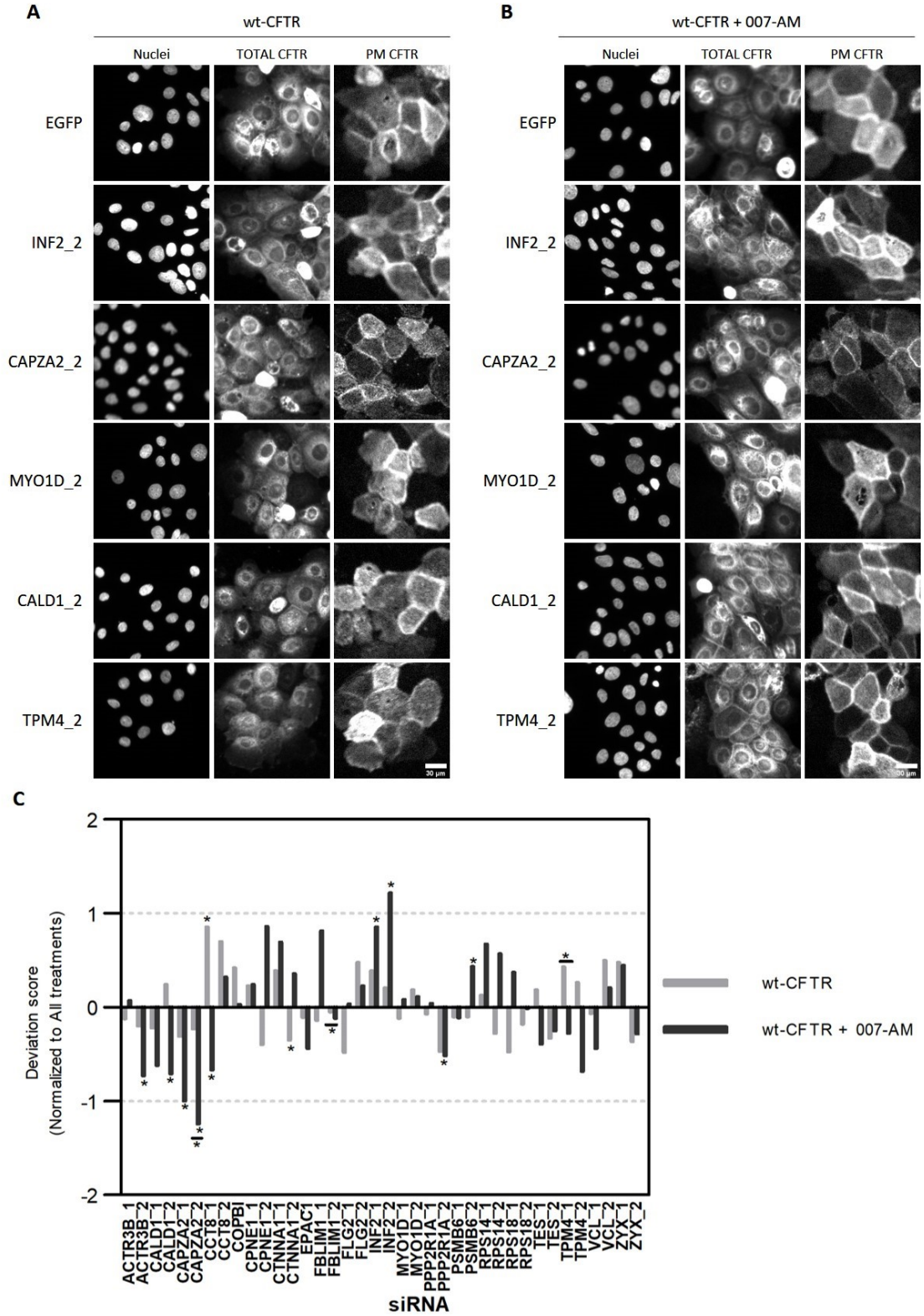

Figure 4: CFTR trafficking efficiency under knockdown of the 19 selected hits. CFBE cell lines expressing mCherry-Flag-wt-CFTR under the control of a doxycycline-inducible promoter were transfected with siRNAs targeting the 19 selected hits. COPB1, EPAC1 and EGFP (non-targeting siRNA) siRNA were used as controls. **A)** Cells were incubated with DMSO (vehicle control) for 2h (representative images). **B)** Cells were incubated with 007-AM (1µM) for 2h. **C)** CFTR trafficking was given by the ratio of PM CFTR (Cy5)/TOTAL CFTR (mCherry). The deviation score was calculated and plotted. Data are shown as the median deviation to all conditions considered. n=3. * $p<0.05$. Statistical analysis was performed using two-tailed unpaired students t-test.

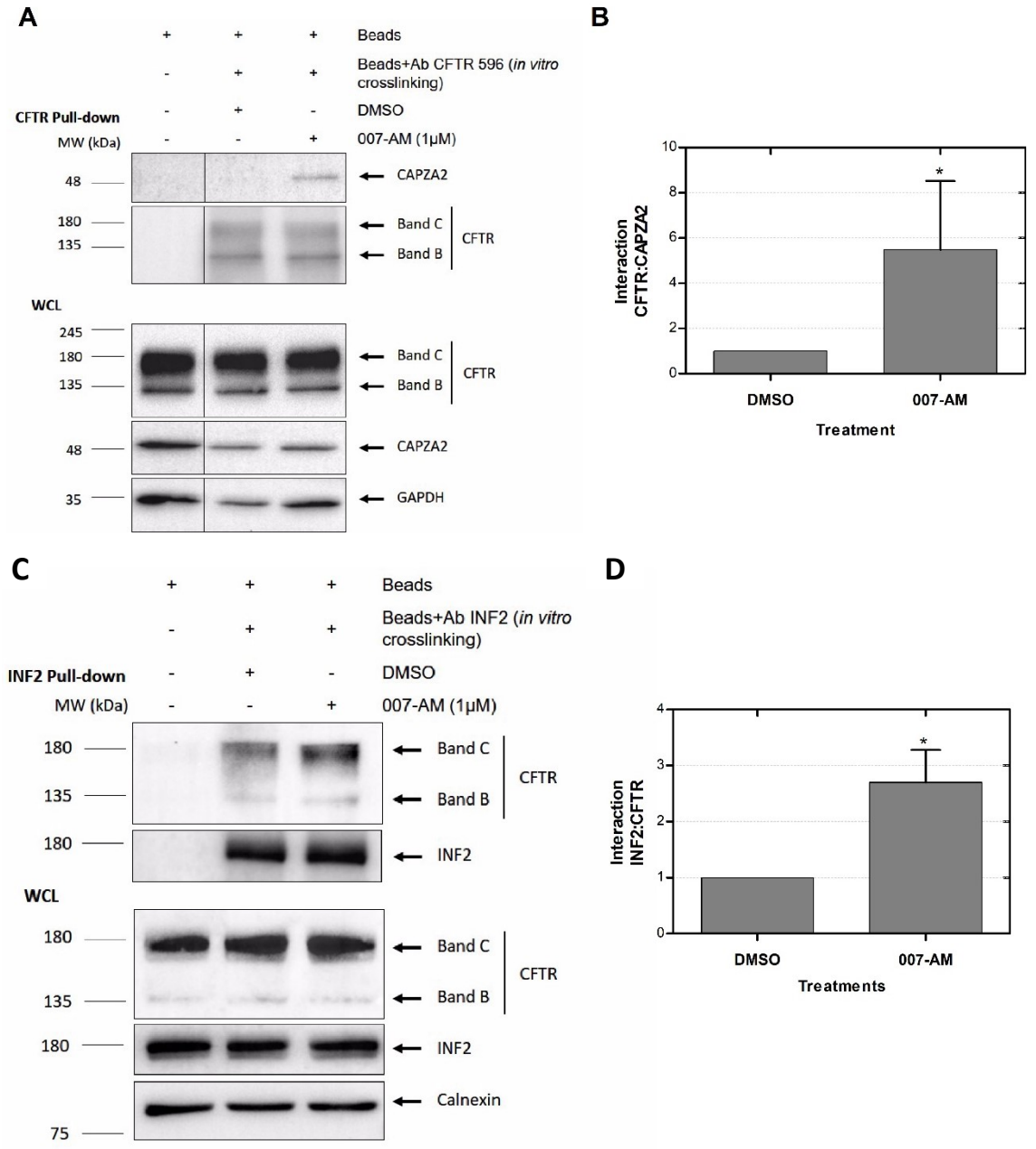

Figure 5: Interaction between CFTR and CAPZA2 or INF2. Co-immunoprecipitation was performed using CFBE cells expressing wt-CFTR incubated with 007-AM (2h, 1 µM) or DMSO (vehicle control). Cell lysates incubated with non-conjugated beads were used as a control. **A)** CAPZA2 was detected by western blot after immunoprecipitation of CFTR (CFTR 596 antibody cross-linked to rProtein G agarose beads). GAPDH was used as the loading control. **B)** Quantification of CFTR:CAPZA2 interaction was performed by calculating the CAPZA2 detected normalized to the amount of immunoprecipitated CFTR. **C)** CFTR was detected by western blot after immunoprecipitation of INF2 (Rabbit polyclonal anti-INF2 antibody cross-linked to rProtein G agarose beads). Calnexin was used as the loading control**. D)** Quantification of INF2:CFTR interaction was performed by calculating the CFTR detected normalized to the amount of INF2 immunoprecipitated. 20% of the total lysate was analysed as WCL. Data are shown as the mean ± SEM, n=3. * $p<0.05$. Statistical analysis was performed using two-tailed unpaired students t-test.

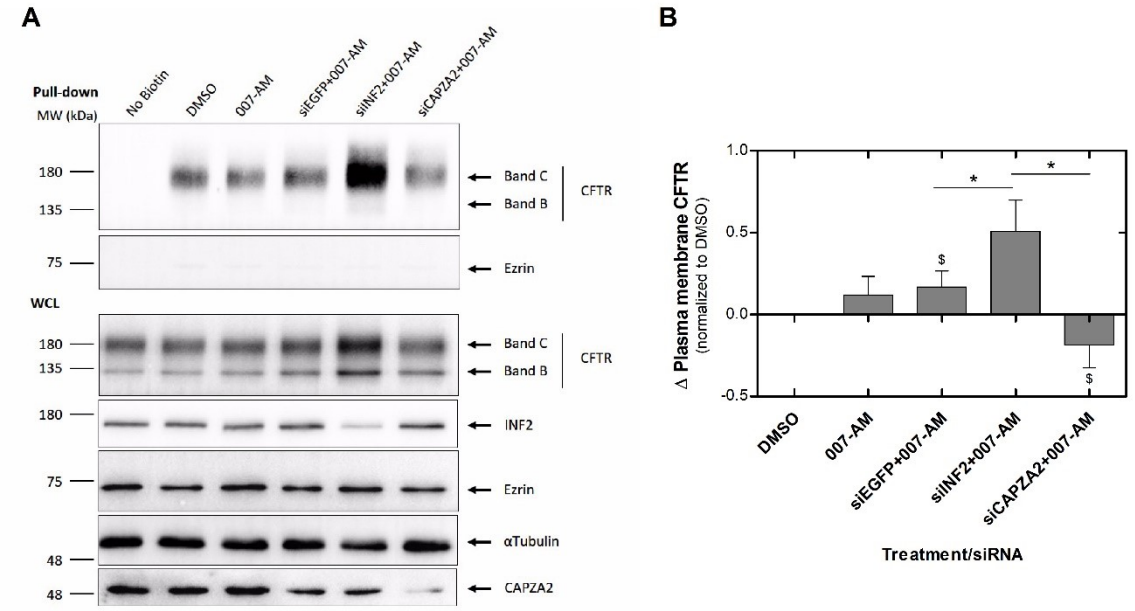

Figure 6: Impact of INF2 and CAPZA2 knockdown in the levels of wt-CFTR at the cell surface under EPAC1 activation. Cell surface biotinylation assay was performed using CFBE cells expressing wt-CFTR transfected with a siRNA against INF2, CAPZA2 or EGFP (non-targeting siRNA) and treated with 007-AM (2h, 1 µM) or DMSO (vehicle control). Cells were incubated with biotin and then cell lysates were incubated overnight with streptavidin beads. Cells not incubated with biotin solution were used as a control. **A)** CFTR was detected by western blot after streptavidin pulled-down. 20% of the total lysate was analysed as WCL. αTubulin was used as the loading control and Ezrin was used as an intracellular protein control. **B)** Quantification of CFTR detected after the pull-down was performed and the change (Δ) normalized to DMSO was plotted. Data are shown as the mean ± SEM, n=3. $ * $p<0.05$. Statistical analysis was performed using two-tailed unpaired students t-test.

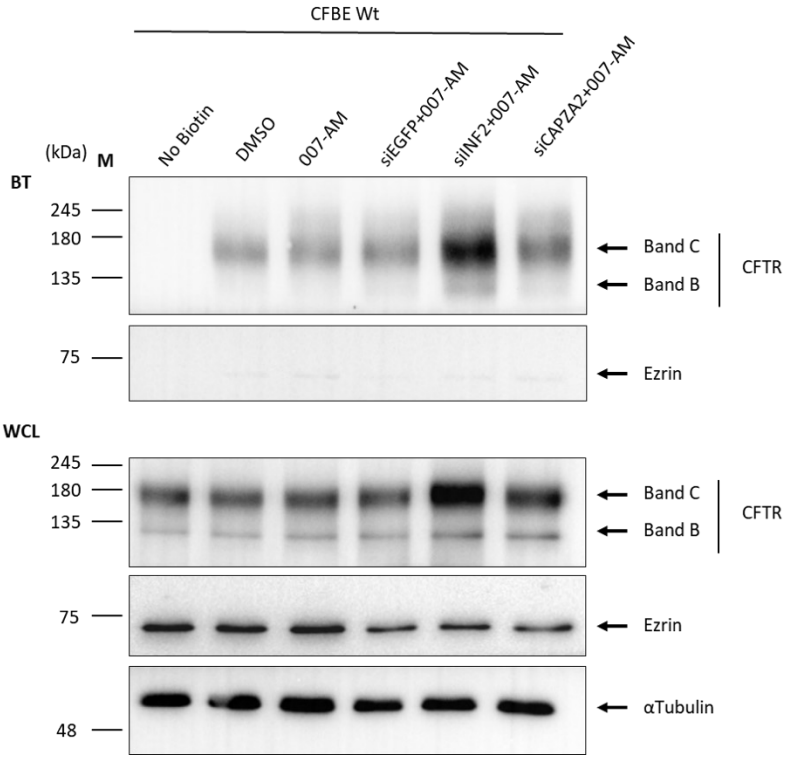

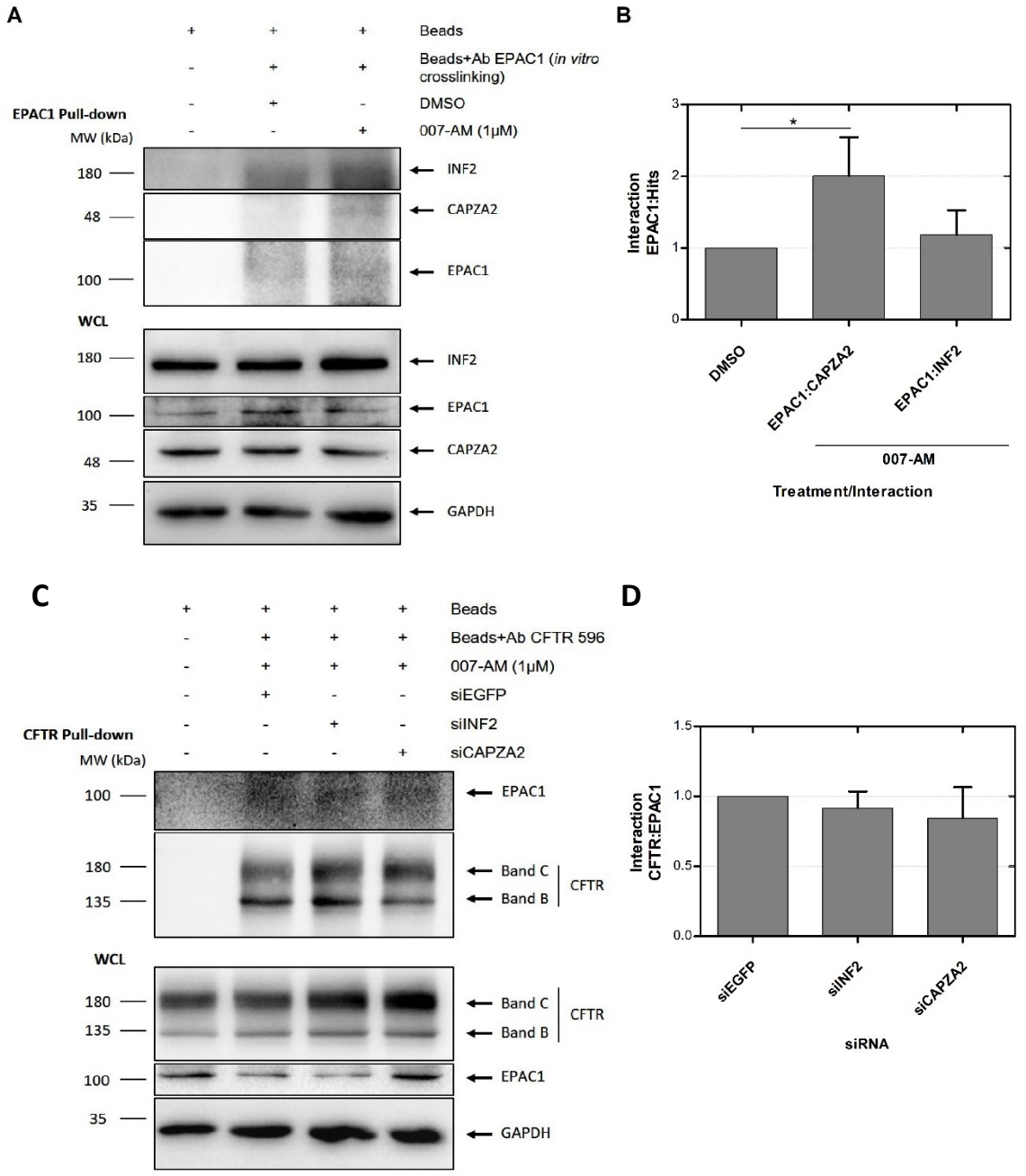

Figure 7: Impact of EPAC1 in CFTR and INF2 or CAPZA2 interaction. Interaction between EPAC1 and CAPZA2 or INF2 were analysed by Co-immunoprecipitation using CFBE cells expressing wt-CFTR incubated with 007-AM (2h, 1 µM) or DMSO (vehicle control). Cell lysates incubated with non-conjugated beads were used as a control. **A)** CAPZA2 and INF2 were detected by western blot after EPAC1 immunoprecipitation. GAPDH was used as the loading control. **B)** Quantification of EPAC1:CAPZA2 or EPAC1:INF2 interaction was performed by calculating the CAPZA2 or INF2 detected normalized to the amount of EPAC1 immunoprecipitated. The impact of INF2 or CAPZA2 knockdown in CFTR:EPAC1 interaction was analysed by Co-immunoprecipitation using CFBE cells expressing wt-CFTR transfected with an siRNA against INF2 or CAPZA2 and incubated with 007-AM (2h, 1 µM). Cell lysates from CFBE cells incubated with non-conjugated beads were used as a control. **C)** EPAC1 was detected by western blot after CFTR immunoprecipitated. GAPDH was used as the loading control. **D)** Quantification of CFTR:EPAC1 interaction was performed by calculating the EPAC1 detected normalized to the amount of CFTR immunoprecipitated. 20% of the total lysate was analysed as WCL. The results are normalized to DMSO and using the mean ± SEM, n=3. * $p<0.05$. Statistical analysis was performed using two-tailed unpaired students t-test.

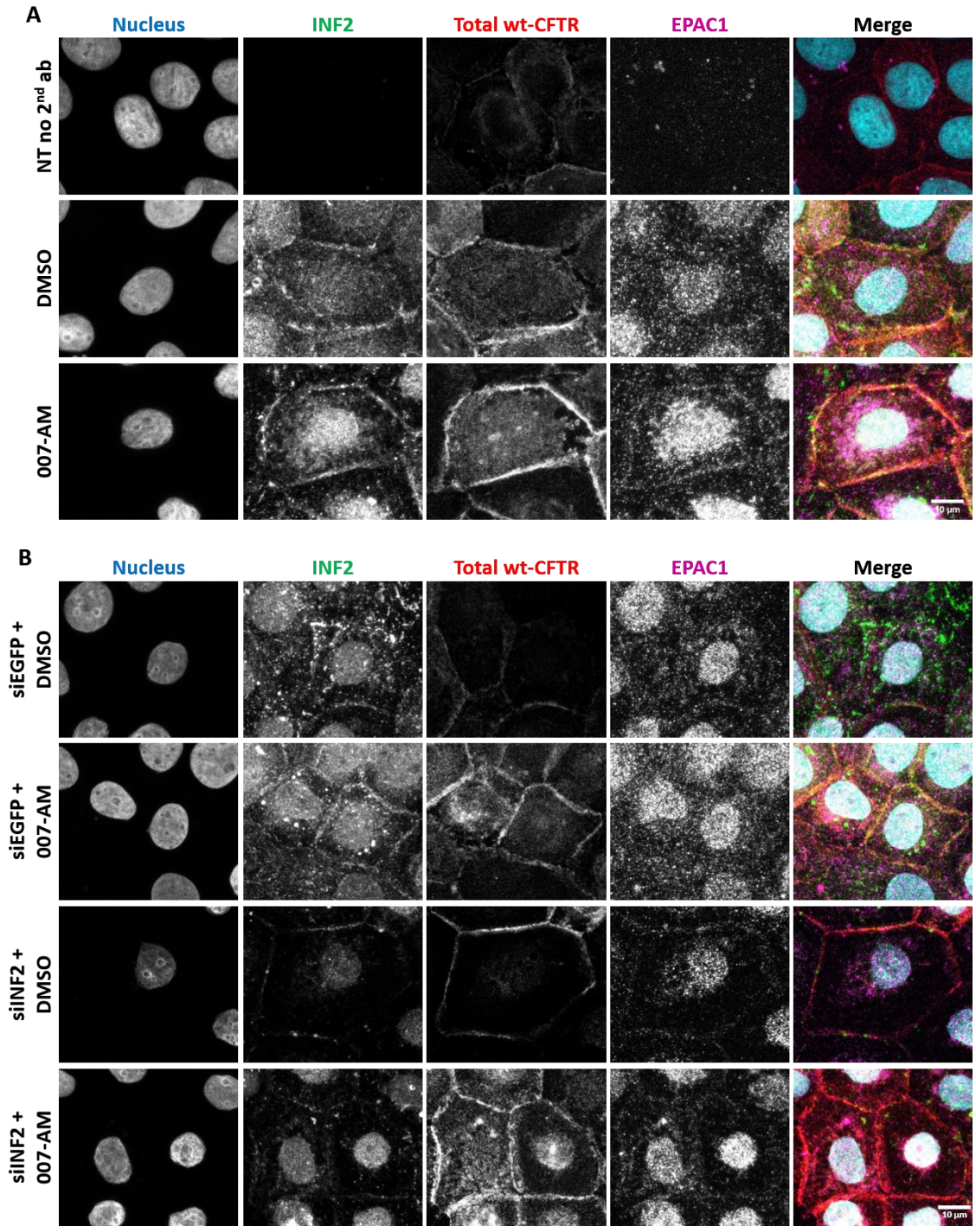

Figure 8: INF2 and EPAC1 expression and localization in CFBE cells expressing wt-CFTR. A) Confocal images showing the expression and localization of INF2 (green), Total wt-CFTR (red) and EPAC1 (magenta) under CFBE cells incubation with 007-AM (1µM, 2h) or DMSO (vehicle control). **B)** Confocal images showing the impact of INF2 (green) knockdown in the levels of EPAC1 (magenta) and Total wt-CFTR (red). CFBE cells expressing wt-CFTR were transfected with an siRNA against INF2 or EGFP (non-targeting siRNA) and incubated with 007-AM (1µM, 2h) or DMSO (vehicle control). After immunostaining, images were acquired on Leica SP8 confocal with 63x oil-immersion objective. Nucleus were stained using Hoechst 33342 (cyan). The scale bar corresponds to 10µm.

Supplementary materials

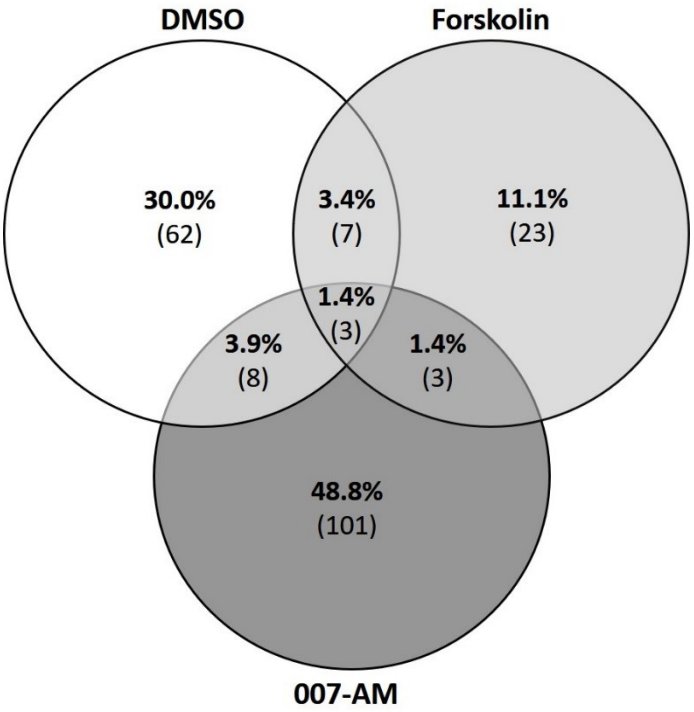

Figure S1: Venn diagram showing the specific CFTR interacting proteins pulled-down under activation of adenylyl cyclase (Forskolin), EPAC1 (007-AM) or DMSO.

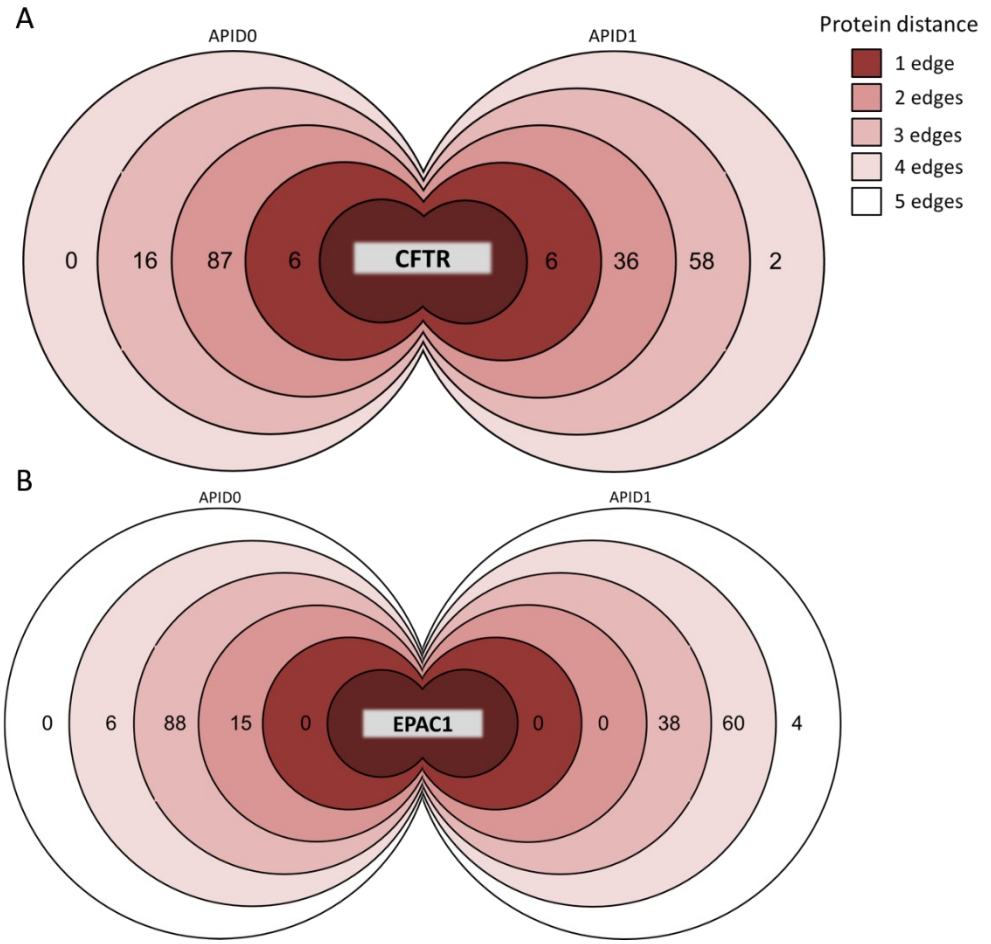

Figure S2: Distance of the 110 interactors under EPAC1 activation to relevant proteins. R programming were used to calculate the distances between proteins APID0 - all known interactions, APID1 - interactions proven by 2 experiments or more. **A)** Distances to CFTR, **B)** Distances to EPAC1.

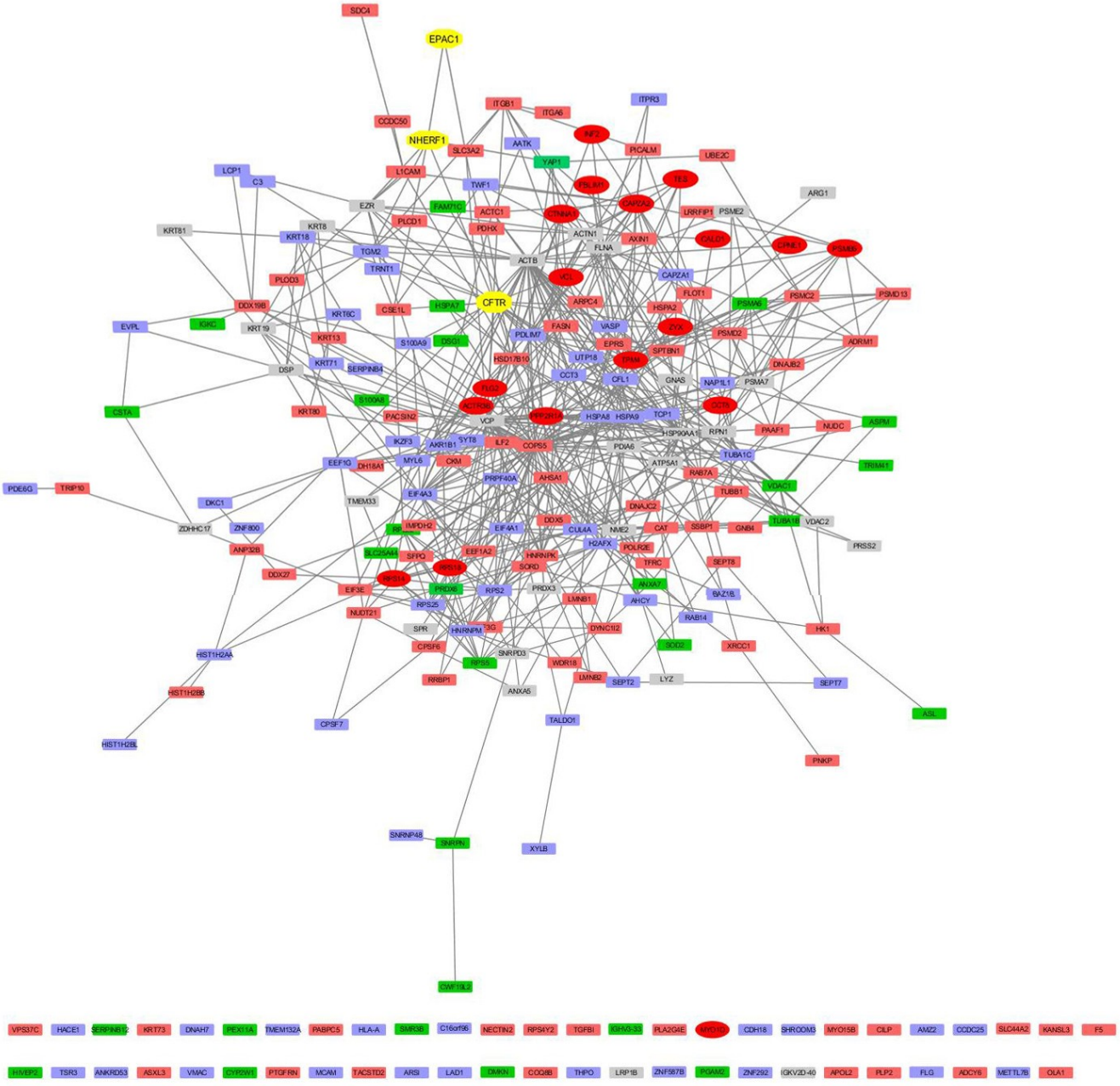

Figure S3 – Protein interaction network for the wt-CFTR interactors identified by nanoLC/MS/MS. The 251 proteins scored with an "interaction score" higher than 2 were considered. NHERF1 and EPAC1 were added to the network. Protein-protein interactions were analysed using APID as the background. Cytoscape was used for visualization of the networks. **Yellow** – Proteins which form a complex involved in CFTR stabilization at the PM (CFTR:NHERF1:EPAC1); **Green** – Specific CFTR interactors under AC stimulation; **Pink** – Specific CFTR interactors under EPAC1 activation; **Blue** – Interactors detected only for the control (DMSO); **Gray** – CFTR interactors identified in several conditions tested; **Red circles** – The 18 hits selected for validation.

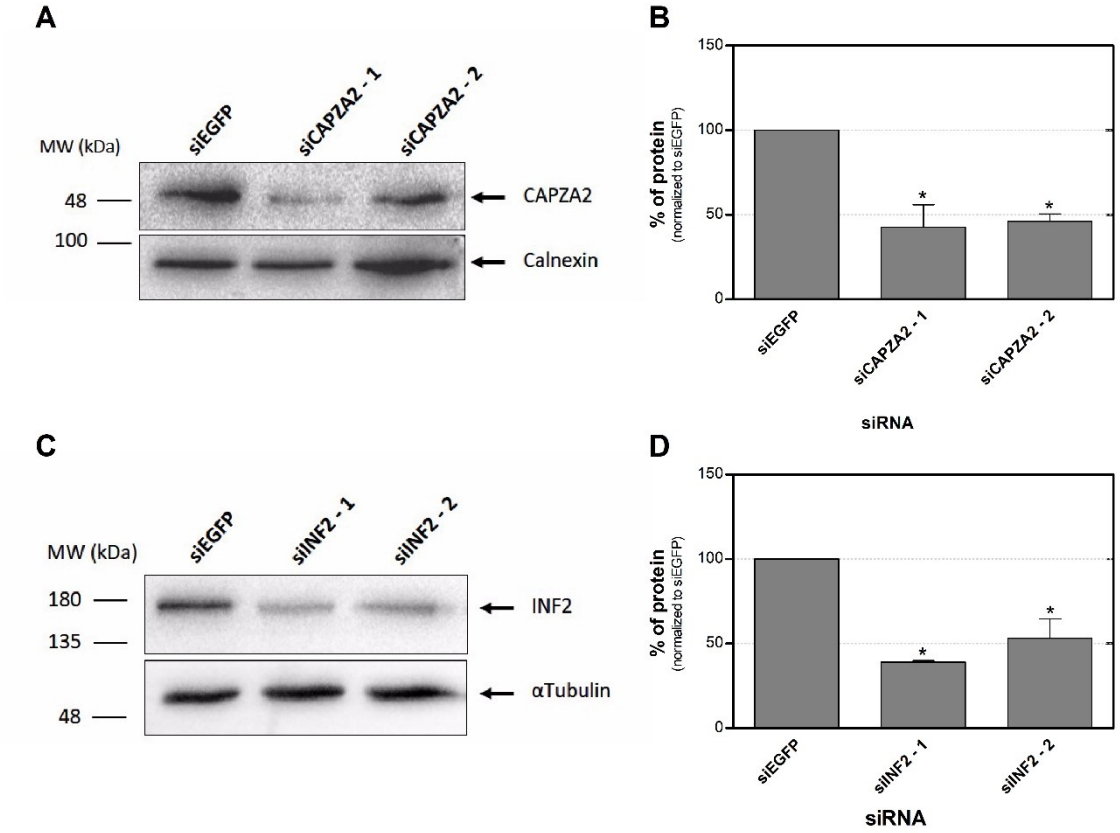

Figure S4: Efficiency knockdowns on CFBE cells expressing wt-CFTR. CFBE cells expressing wt-CFTR were transfected with 2 siRNAs against CAPZA2, INF2 or EGFP as non-targeting siRNA for 48h. **A)** Detection of CAPZA2 (top) and Calnexin (bottom) which was used as the loading control. **B)** Quantification of the levels of CAPZA2 normalized to siEGFP. **C)** Detection of INF2 (top) and αTubulin (bottom) which was used as the loading control. **D)** Quantification of the levels of INF2 normalized to siEGFP. Data are shown as the mean ± SEM, n=2. * $p<0.05$. Statistical analysis was performed using two-tailed unpaired students t-test.

Table S1 – Confidence Score. Definition and criteria for protein scoring.

Table S2 – List of siRNAs used for target knock-down.

Table S3 – Full list of identified proteins. A – complete set. B – proteins identified as interactors of wt-CFTR in cells treated with DMSO, Fsk or 007-AM or under control conditions (parental cells and cells expressing wt-CFTR incubatedonly with beads).

Table S4 – Lists of specific proteins. A – complete set. B – proteins identified for each condition (DMSO, Fsk or 007-AM).

Table S5 – Confidence scores of the proteins identified for each condition (DMSO, Fsk or 007-AM).

Table S6 – Selected hits.

Table S7 – List of specific proteins used for network generation.